JOURNAL OF PETROLOGY | VOLUME 37 | NUMBER 6 | PAGES 1409–1436 | 1996

JEFFREY H. TEPPER*

DEPARTMENT OF GEOLOGICAL SCIENCES, UNIVERSITY OF WASHINGTON, SEATTLE, WA 98195, USA, AND GEOLOGY DEPARTMENT, UNION COLLEGE, SCHENECTADY, NY 12308, USA

Petrology of Mafic Plutons Associated with Calc-Alkaline Granitoids, Chilliwack Batholith, North Cascades, Washington

Small (<5 km^2), lithologically diverse gabbro and diorite stocks make up ~2% of the 34 to 2 Ma Chilliwack batholith, and overlap in age with associated calc-alkaline granitoids. These mafic plutons are similar to those in other I-type batholiths, and represent basaltic magmas present during batholith formation. Objectives of this study are: (1) to examine the origins of both interpluton and intrapluton petrologic diversity, and (2) to compare chemical and Sr–Nd isotopic traits of these gabbros with those of Cascade arc basalts. Mafic rocks in the Chilliwack are divided into a medium-K series (MKS) and a low-K series (LKS). The former contain 0·7–2·4 wt % K_2O and are similar in composition to calc-alkaline basalts and basaltic andesites. Inverse REE modeling supports derivation of the MKS by 9–27% melting of a garnet-free, LREE-enriched source ($La/Yb_N \sim 2$). Chilliwack LKS gabbros have chemical characteristics of low-K olivine tholeiites, including low K_2O (0·3–0·5 wt %) and La/Yb_N (1·7–3·4), and high CaO (8·8–11·3 wt %) and Na_2O/K_2O (6–22). These traits suggest a source with more clinopyroxene and lower La/Yb_N than the MKS source. Differences in $\varepsilon_{Nd(0)}$ between MKS and LKS gabbros suggest that lower Nd/Sm is a long-lived LKS source characteristic. Lithologic variation within composite plutons of both series resulted primarily from multiple intrusion of related magmas, in some cases differentiates of a common parent. Two contrasting examples were studied in detail. At Mt Sefrit, MKS variation (gabbronorite–quartz diorite) is modeled by low-pressure fractionation (ol + plag + cpx), accompanied by ~10% wallrock assimilation. In contrast, chemical and Sr–Nd isotopic variation among LKS gabbro–quartz diorite at Copper Lake points to crystallization dominated by clinopyroxene + plagioclase ± Cr-spinel, indicative of differentiation at pressures ⩾10 kbar, although the assimilant in this case is poorly constrained. Chemical and isotopic similarities between these mafic plutons and Quaternary Cascade lavas indicate that mafic magmas present during the production of Chilliwack granitoids were low- and medium-K arc basalts.

KEY WORDS: *arc magmatism; Cascades; gabbro; granitoid; trace element*

INTRODUCTION

For at least two billion years subduction zone magmatism has been one of the dominant processes by which new continental crust is generated. Although our understanding of the process remains incomplete, it is clear that basaltic magmas play a fundamental role, transferring both heat and mass from the mantle to the crust. Mantle-derived magmas are represented in most continental arc batholiths by gabbroic plutons, synplutonic mafic dikes, and/or mafic inclusions within the granitoids, and an understanding of their origin and evolution is crucial for deciphering the origin(s) of the associated granitoids. For this reason, mafic inclusions in I-type granitoids have received much attention (Reid *et al.*, 1983; Blundy & Sparks, 1992), but in general these have been extensively modified by interaction with the host granitoids, such that their original geochemical characteristics are obscured (Eberz & Nicholls, 1990). By comparison, mafic plutons are in most cases less contaminated and thus provide a clearer window through which to study the petrogenesis of mantle-derived magmas present during batholith formation.

Mafic plutons in I-type batholiths typically display great diversity in mineral assemblage, texture, and chemical composition, and previous studies have emphasized the importance of fractional

*Present address: Department of Physics, Astronomy, & Geology, Valdosta State University, Valdosta, GA 31698, USA.
Telephone: (912) 249-4847 or 333-5752. Fax: (912) 333-7389.
e-mail: jtepper@valdosta.peachnet.edu

crystallization, subsolidus modification, and depth of emplacement in producing this diversity (Miller, 1937; Mullan & Bussell, 1977; Walawender & Smith, 1979; Regan, 1985; Beard & Day, 1988). However, few studies of continental arc gabbros have examined the importance of source heterogeneity and/or sub-crustal processes, although the importance of these factors is widely acknowledged in explaining the geochemical diversity of arc basalts (Leeman *et al.*, 1990). This study of the mafic stocks in the Chilliwack batholith, North Cascades, focuses on two distinct types of geochemical and isotopic diversity: differences between plutons (interpluton variation) and diversity within individual composite stocks (intrapluton variation). A major goal is to improve understanding of the relative contributions of source heterogeneity, degree of melting, and differentiation processes (fractional crystallization, assimilation) to both types of diversity.

Study of Chilliwack gabbros also affords the opportunity to compare Oligocene–early Miocene mafic magmas from the Northern Cascades with Miocene–Recent basaltic rocks from the Central and Southern Cascades. The younger basalts display wide variations in chemical and isotopic composition that have been attributed to magma generation from heterogeneous mantle containing both ocean-island basalt (OIB) and mid-ocean ridge basalt (MORB) source domains, and to variable involvement of a slab-derived subduction component and/or asthenospheric mantle (Bacon, 1990; Hughes, 1990; Leeman *et al.*, 1990; Clynne, 1993). In some cases, basalt composition has been related to tectonic setting and/or crustal structure, as in the case of low-K olivine tholeiites, which are associated with areas of extension (Bacon, 1990). Because volcanic cover is scarce in the Northern Cascades, none of these previous studies have included basalts from this part of the arc. Geochemical and isotopic data from Chilliwack gabbros thus offer an initial opportunity to evaluate spatial as well as temporal variations in magma composition that may reflect contrasts in source and/or tectonic regime.

GEOLOGIC SETTING

During the past ~38 Ma the Cascade Range has been a site of arc magmatism related to subduction of the Juan de Fuca plate system beneath western North America. In the North Cascades, Plio-Pleistocene uplift and erosion have removed most of the volcanic cover, exposing a chain of epizonal, calc-alkaline batholiths. The largest of these is the ~960 km^2 Chilliwack batholith (Fig. 1), which contains dozens of individual plutons that were emplaced between 36 and 2 Ma into a diverse assemblage of pre-Tertiary metamorphic rocks and subordinate Tertiary volcanic and sedimentary units. Misch (1966) grouped the pre-Tertiary rocks into three structural–metamorphic provinces: (1) the Northwest Cascades Thrust System; (2) the Skagit Crystalline Core; (3) the Methow–Pasayten belt (Fig. 1). These provinces are now recognized as containing several allochthonous terranes that were assembled during a Late Cretaceous contractional orogeny, and subsequently dissected by Tertiary strike-slip faulting (McGroder, 1991). The Chilliwack intrudes rocks of all three provinces, and plugs the faults between them (Fig. 1). From west to east, major host units for the Chilliwack include: (1) Darrington Phyllite and Shuksan Greenschist of the Jurassic Shuksan Suite, which is the uppermost nappe in the Northwest Cascades Thrust System; (2) greenschist to amphibolite-facies ortho- and paragneisses of the Skagit Complex, which yield Cretaceous to Eocene ages of metamorphism; (3) Jurassic and younger oceanic sedimentary rocks and greenstone units of the Hozomeen Group. Some Chilliwack plutons also intrude Cascade arc volcanics (Brown *et al.*, 1987).

Individual Chilliwack plutons range from <1 km^2 to >100 km^2 in area. Their dominant lithologies are granodiorite and tonalite, although for the batholith as a whole the range of rock types is from gabbro to granite (*sensu stricto*). Emplacement depths of less than ~10 km are inferred for all plutons on the basis of narrow contact aureoles, local intrusion into coeval volcanic units, and the results of hornblende barometry on the granitoid rocks, which indicate crystallization at $P<3$ kbar (Tepper, 1991). The granitoid rocks and their relationships to the mafic rocks have been described previously (Tepper *et al.*, 1993).

FIELD RELATIONS, GEOCHRONOLOGY, AND PETROGRAPHY

Eleven mafic stocks, having a combined area of ~19 km^2, have been recognized in the Chilliwack, and represent ~2% of the total exposed area. These gabbros and diorites are scattered throughout the batholith, but are most common along the margins, near roof pendants, and as satellite stocks (Fig. 1). Where contacts between mafic rocks and granitoids are exposed, intrusive relations consistently indicate that the mafic stocks predate all granitoid plutons in the immediate vicinity. However, for the batholith as a whole there is significant overlap between

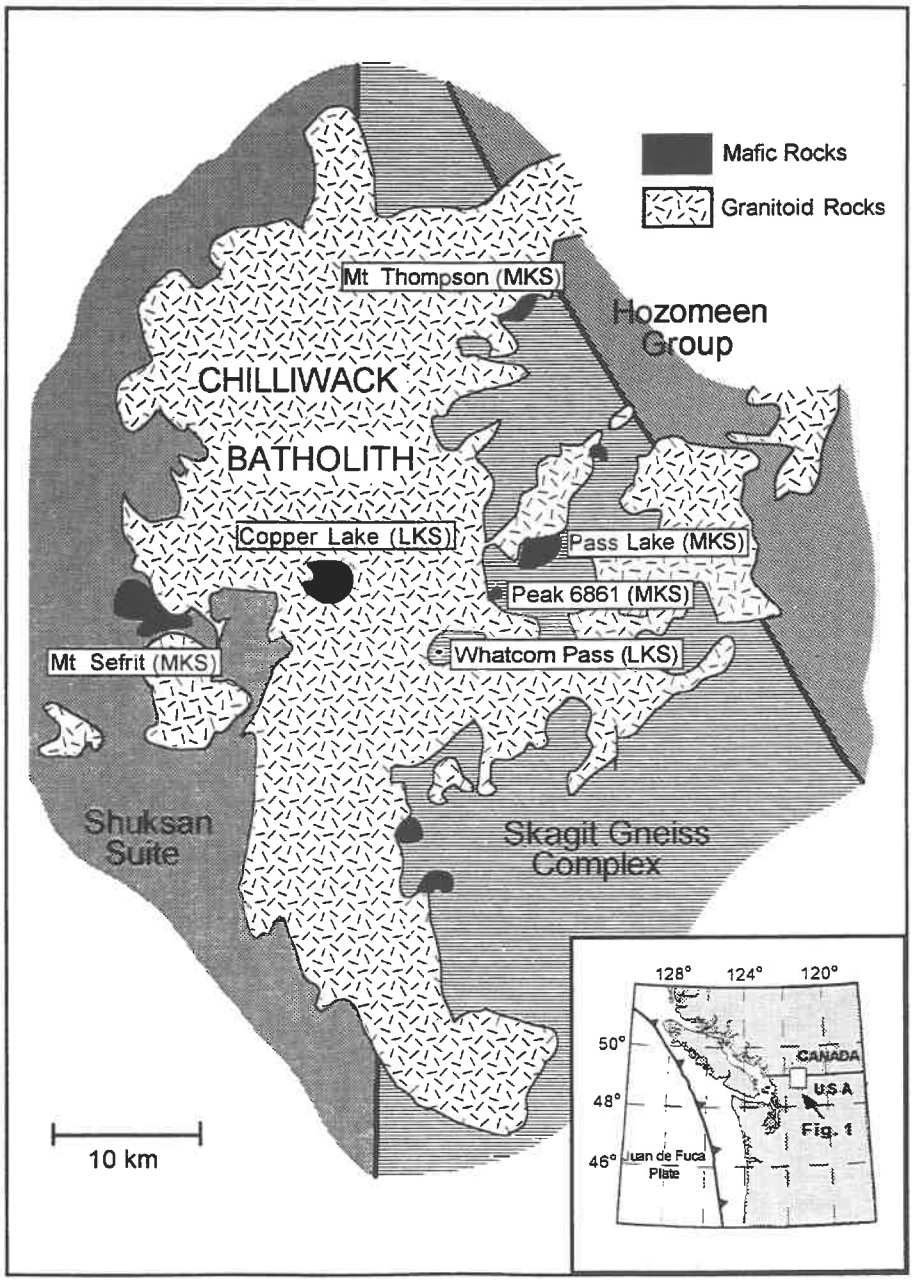

Fig. 1. Simplified geologic map of the Chilliwack batholith and its host rocks. Mafic plutons included in this study are labeled (MKS, medium-K series; LKS, low-K series). Bold lines separating host rock units are faults. Volcanic rocks and surficial deposits are not shown, nor are the boundaries of individual granitoid plutons within the batholith. Geology compiled from Tepper (1991), Richards (1971), and R. Tabor & R. Haugerud (US Geological Survey, personal communication, 1995).

radiometric ages of mafic rocks (34–22 Ma) and those of granitoid plutons (35–2 Ma). The gabbros and diorites are interpreted to represent small batches of mafic magma that locally preceded the more voluminous granitoid magmas. This sequence, gabbro followed by granitoid, occurred at different times in different areas of the batholith, but mafic and granitoid magmatism clearly do not represent separate time intervals in the history of the batholith.

Lithologic diversity, a characteristic feature of mafic stocks in the Chilliwack, is manifest at both outcrop and interpluton scale. Outcrop-scale heterogeneities include modal layering, pockets of unusually fine- or unusually coarse-grained minerals, monomineralic segregations, net veining, and dikes.

These within-pluton structures probably resulted from crystal–liquid separation, local build-up of dissolved water, and/or multiple intrusive events involving cogenetic magmas. Similar features are observed among gabbros in other calc-alkaline batholiths (Larsen, 1948; Bateman, 1983; Regan, 1985). At the interpluton scale, however, Chilliwack gabbros display differences in chemical and isotopic composition that suggest they originated from dissimilar parent magmas. On this basis, mafic plutons in the Chilliwack are subdivided into a Medium-K series (MKS) and a Low-K series (LKS).

Medium-K series (MKS)

The medium-K series is the more widespread of the two (Fig. 1), and consists of gabbronorites, gabbros, diorites, and quartz diorites that bear many similarities to pyroxene-bearing mafic plutons in other calc-alkaline batholiths (Miller, 1937; Erickson, 1977; Fourcade & Allègre, 1981; Fabries *et al.*, 1984; Regan, 1985; Beard & Day, 1988). The largest MKS pluton is the ~ 6 km^2 Mt Sefrit Gabbronorite, dated by a four-point Rb/Sr mineral–whole rock isochron at $22{\cdot}85 \pm 0{\cdot}05$ Ma (Tepper, 1991). This pluton consists of at least four separate phases that show a progression toward more evolved compositions with decreasing age (olivine gabbronorite ⇒ pyroxene diorite ⇒ hornblende diorite ⇒ biotite–hornblende quartz diorite). Contacts between phases vary from sharp to gradational, but there is little evidence of chilled margins or contact metamorphism even at sharp contacts, suggesting that the time between pulses was relatively short. In contrast, the external contact of the pluton with the host Darrington Phyllite is marked by a narrow zone of intrusion breccia, and fine-grained gabbronorite at the summit of Mt Sefrit is interpreted as part of a chilled margin that formed against the now-eroded roof of the stock. Contact metamorphism of the phyllite (hypersthene–cordierite hornfels at the contact) extends outward only tens of meters from the pluton.

Other MKS plutons in the Chilliwack contain rock types similar to those at Mt Sefrit, and also commonly show evidence of multiple intrusions. The plug of gabbronorite and gabbro at Pass Lake contains synplutonic dikes and enclaves of two-pyroxene diorite. Similarly, two-pyroxene diorite at Peak 6861 is cut by discontinuous dikes of gabbronorite porphyry and surrounded by an intrusion of biotite–hornblende quartz diorite.

The majority of MKS samples are fine to medium grained and hypidiomorphic, and typically contain 50–70% plagioclase, 15–30% mafic silicates, and lesser amounts of interstitial quartz, alkali feldspar, and opaque oxides. The plagioclase commonly displays patchy zoning (Vance, 1965) consisting of a partially resorbed calcic core (An_{87-60}) overgrown and infilled by an oscillatory–normal zoned sodic mantle (An_{56-33}). The abrupt compositional break between core and mantle averages ~ 15 An %, but is as great as 39 An % in some grains. Olivine (Fo_{74-65}) is rare; it occurs only as phenocrysts in the chilled margin and as inclusions within pyroxene at Mt Sefrit, although several other MKS plutons contain orthopyroxene–magnetite symplectites that probably formed by subsolidus oxidation of olivine. Gabbronorites contain augite ($Wo_{43}En_{46}Fs_{11}$–$Wo_{42}En_{40}Fs_{18}$) and hypersthene ($Wo_3En_{70}Fs_{27}$–$Wo_2En_{59}Fs_{39}$) in subequal amounts, both commonly with amphibole rims. Temperatures obtained from coexisting pyroxenes range from 967 to 1020°C (Table 1). Augites from Mt Sefrit (Table 2, Nos 2–4) show a positive correlation between Al_2O_3 content ($1{\cdot}1$–$5{\cdot}0$ wt %) and *mg*-number [mol % Mg/(Mg + Fe)], and the more magnesian crystals (*mg*-numbers $> 0{\cdot}78$; average $Al_2O_3 = 3{\cdot}6$ wt %; average CaO = $21{\cdot}5$ wt %) are similar in composition to augites crystallized in basaltic liquids at 1–2 kbar P_{H_2O} (Sisson & Grove, 1993). These aluminous augites at Mt Sefrit are out of Fe–Mg equilibrium with coexisting olivine and orthopyroxene and are probably xenocrysts that crystallized at higher P_{H_2O}. Amphiboles in the MKS are of two types: (1) magnesio-hornblendes that occur as magmatic overgrowths on pyroxene and as interstitial grains; (2) titaniferous tschermakite oikocrysts [amphibole nomenclature of Leake (1978)]. Both types may occur in the same sample. At Mt Sefrit, with increasing differentiation (gabbronorite–quartz diorite), the magnesio-hornblendes become more abundant and show a decrease in Ca and *mg*-number, and an increase in Ti, Al, Mn, Na, and K (Fig. 2). Individual grains commonly display zoning, which may or may not mimic the trends defined by the MKS as a whole. The tschermakite oikocrysts, which occur near the contact between the Mt Sefrit gabbronorite and a younger quartz diorite, are distinguished by high Ti and Na contents (Table 3, No. 2; Fig. 2) and may have crystallized from trapped melt. Similar oikocrysts in olivine gabbros and mafic gabbronorites from the Smartville Complex have been interpreted as being near- or sub-solidus (Beard & Day, 1988). Growth of amphibole late in the crystallization interval at Mt Sefrit is also reflected in amphibole–plagioclase thermometry (Table 1), which yields temperatures 300–350°C lower than those obtained from pyroxene pairs. Biotite occurs in the MKS as overgrowths and interstitial grains, and constitutes up to 10% of some samples. Orthoclase

Table 1: Geothermometry results for MKS and LKS plutons

Pluton (series):	Mt Sefrit (M)	Mt Sefrit (M)	Copper Lake (L)	Copper Lake (L)	Copper Lake (L)
Rock type:	gabbronorite	qtz diorite	gabbro	diorite	qtz diorite
Sample no(s):	82-007, -046, -053	82-104	88-022	87-109	87-112, 88-053
cpx–opx*	967–1020†	–	843	–	920§
amph–plag 1†	669	705	785	838	770
amph–plag 2‡	651	718	—	—	763

Temperatures (°C) calculated with: *cpx–opx thermometer of Wells (1977), and †edenite–tremolite–plagioclase and ‡edenite–richterite–plagioclase thermometers of Holland & Blundy (1994). Accuracies of these thermometers estimated by authors to be ± 70°C, ± 40°C, and ± 40°C, respectively. §Cpx–opx temperature obtained on sample from chilled margin of pluton; all other temperatures obtained on samples from pluton interiors.

Table 2: Representative clinopyroxene analyses

Analysis:	1	2	3	4	5	6	7
Pluton:	Whatcom (L)	Sefrit (M)	Sefrit (M)	Sefrit (M)	Copper L. (L)	Copper L. (L)	Copper L. (L)
Rock type:	hbldite	gab-nor	gab-nor	gab-nor	hb gabbro	hb diorite	px diorite
Sample no.:	87-036	82-046	82-046	82-046	88-022	87-109	88-053
SiO_2	52·25	51·10	51·72	51·37	52·44	51·71	51·02
TiO_2	0·32	0·73	0·62	0·57	0·17	0·20	0·22
Al_2O_3	3·81	3·69	1·49	1·30	0·66	0·95	0·83
Cr_2O_3	na	0·18	0·05	0·02	0·00	0·00	0·00
FeO	5·62	7·25	10·10	10·59	9·46	9·80	13·62
MnO	0·15	0·19	0·26	0·26	0·34	0·44	0·55
MgO	16·05	15·90	14·74	14·60	13·94	14·37	12·75
CaO	21·47	20·96	20·87	20·69	22·35	21·78	20·47
Na_2O	0·25	0·38	0·30	0·33	0·27	0·25	0·28
Total	99·92	100·37	100·13	99·73	99·63	99·49	99·73
Cations per 6 oxygens							
Si	1·92	1·89	1·94	1·94	1·97	1·95	1·95
Ti	0·01	0·02	0·02	0·02	0·01	0·00	0·00
Al	0·17	0·16	0·07	0·06	0·03	0·04	0·04
Cr	0·00	0·01	0·00	0·00	0·00	0·00	0·00
Fe^{2+}	0·17	0·22	0·32	0·33	0·30	0·31	0·44
Mn	0·01	0·01	0·00	0·01	0·01	0·01	0·02
Mg	0·88	0·87	0·82	0·82	0·78	0·81	0·73
Ca	0·84	0·83	0·84	0·84	0·90	0·88	0·84
Na	0·02	0·03	0·02	0·02	0·02	0·02	0·02
Σ cations	4·01	4·03	4·03	4·04	4·02	4·03	4·04
Wo	44·6	43·0	42·4	42·0	45·5	44·1	41·9
En	46·3	45·4	41·6	41·2	39·5	40·4	36·3
Fs	9·1	11·6	16·0	16·8	15·0	15·5	21·8
mg-no.	83·6	79·6	72·2	71·1	72·4	72·3	62·5

Abbreviations for rock types and pluton names listed in Table 4 except hbldite (hornblendite xenolith). na = not analyzed.

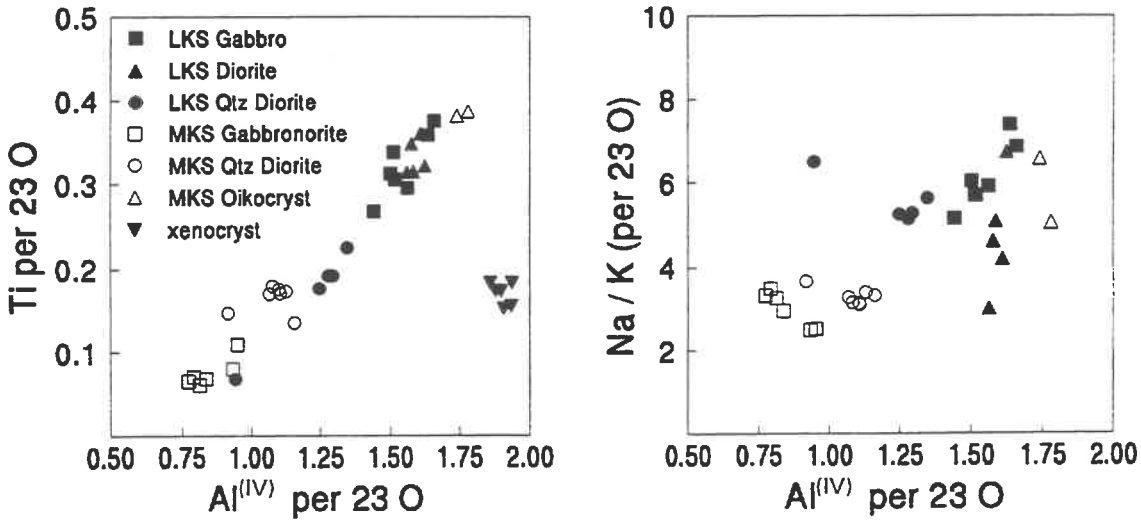

Fig. 2. Plots of Ti vs $Al^{(IV)}$ and Na/K vs $Al^{(IV)}$ illustrating diversity of amphibole compositions in Chilliwack samples. Symbols indicate different rock types. Tschermakite xenocrysts have Na/K > 20 and are not shown on the second plot.

($Or_{86}Ab_{13}An_1$) is also interstitial, but seldom exceeds 2% of the mode. Ilmenite, partially replaced by magnetite, occurs as early formed grains and as a breakdown product of primary mafic silicates. Primary magnetite occurs with ilmenite in the more differentiated rocks. Apatite and zircon are common accessories, pyrrhotite and sphene are less common, the latter being late formed and restricted to samples containing amphibole oikocrysts. Based on textural evidence, the inferred MKS crystallization sequence is olivine ⇒ augite ≈ plagioclase ⇒ hypersthene ⇒ hornblende ⇒ biotite ⇒ quartz ⇒ orthoclase.

Low-K series (LKS)

The low-K series is represented by the 4 km^2 Copper Lake Gabbro, and by a cluster of small stocks near Whatcom Pass (Fig. 1). A hornblende diorite dike 7 km west of Copper Lake also belongs to this series. The Copper Lake Gabbro, dated by a four-point Rb/Sr mineral–whole rock isochron at 34·0 ± 0·9 Ma (Tepper, 1991), consists of a 0·1 km^2 body of oikocrystic hornblende gabbro, surrounded and intruded by several pulses of equigranular hornblende diorite. The diorites have in turn been intruded by younger granitoid plutons, and thus no original diorite–wallrock contacts were observed. The contact between gabbro and diorite is sharp and steeply dipping, and in places a narrow chilled margin is developed in the younger diorite. However, it appears that elsewhere the older gabbro was still hot and plastic when intruded by the diorite. Locally within the diorite there is a subtle zonation to quartz diorite, defined by an inward increase in biotite and quartz content, an inward decrease in pyroxene content, and progressively earlier crystallization of amphibole. This zoning probably developed *in situ* as the diorite solidified from its margins inward. Both the gabbroic and dioritic units of this stock contain hornblende pegmatite segregations (hornblende + plagioclase + quartz ± apatite ± biotite ± sulfides ± epidote) up to 40 cm long. A notable feature of diorite dikes and pluton margins at Copper Lake is the lack of porphyritic textures, which suggests that these magmas were largely liquid at the time of emplacement.

Most LKS stocks at Whatcom Pass are heavily altered, and only one has been studied in detail. This small plug (0·01 km^2) consists of three phases, which are, in order of decreasing age: (1) xenolith-rich marginal gabbronorite, containing amphibole megacrysts and inclusions of gabbro, hornblendite, and orthogneiss; (2) two-pyroxene diorite porphyry; (3) biotite–hornblende quartz diorite. The gabbroic xenoliths in phase (1) are up to 60 cm in diameter and may represent an earlier unit of this stock that is not exposed. Petrographically, the LKS rocks at Whatcom Pass are similar in texture, color index, and mineral assemblage to MKS rocks, but contain no alkali feldspar.

The LKS pluton at Copper Lake differs from all other mafic stocks in the Chilliwack in that hornblende is the dominant mafic mineral. The gabbro at Copper Lake has a medium-grained orthocumulate texture and contains 50–70% cumulus plagioclase, 20–40% intercumulus amphibole, minor pyroxene, and only trace amounts of biotite, apatite, ilmenite, and pyrrhotite. Copper Lake diorites are fine to

Table 3: Representative amphibole analyses

Analysis:	1	2	3	4	5	6	7		8	9
Pluton:	Sefrit (M)	Sefrit (M)	Sefrit (M)	Copper Lake (L)	Copper Lake (L)	Copper Lake (L)	Whatcom (L)		Copper Lake (L)	dike (L)
Rock type:	gab-nor	gab-nor	qtz diorite	gabbro	diorite	qtz diorite	gab-nor		diorite	diorite
Sample no.:	82-053	82-061	82-104	88-022	87-109	87-112	87-036		87-109	83-011
Comment:	rim on px	oikocryst		oikocryst			xenocryst			
SiO_2	50·25	42·99	47·59	44·09	43·35	46·27	43·11	Sc	91·9	86·8
Al_2O_3	4·99	10·91	5·89	9·83	10·08	7·22	13·67	Cr	6·8	1·3
TiO_2	0·71	3·53	1·51	2·92	2·98	1·55	1·60	Co	59·5	40·7
FeO	13·04	11·78	16·66	14·93	16·44	20·26	9·29	Cs	0·21	0·33
MgO	15·84	14·12	13·06	12·26	11·05	10·38	15·84	Sr	130	160
MnO	0·21	0·20	0·39	0·22	0·28	0·46	0·13	Ba	116	135
CaO	11·11	11·30	10·64	11·47	11·15	10·68	11·37	La	8·2	4·3
Na_2O	0·71	1·87	1·12	1·73	1·43	1·06	2·08	Ce	28·3	17·8
K_2O	0·36	0·50	0·52	0·43	0·48	0·29	0·16	Sm	8·71	7·88
F	na	0·10	na	na	0·05	na	0·08	Eu	2·57	2·48
OH=F	0·00	–0·04	0·00	0·00	–0·01	0·00	–0·02	Tb	1·77	1·62
Total	97·22	97·23	97·38	97·88	97·28	98·17	97·30	Yb	5·26	5·18
								Lu	0·69	0·70
								Ta	0·36	0·20
								Hf	3·57	2·77
Cations based on 23 O										
Si	7·15	6·24	6·92	6·45	6·41	6·78	6·10			
$Al^{(IV)}$	0·84	1·76	1·01	1·55	1·59	1·22	1·90			
$Al^{(VI)}$	0·00	0·11	0·00	0·15	0·17	0·03	0·38			
Ti	0·08	0·38	0·16	0·32	0·33	0·17	0·17			
Fe^{2+}	1·55	1·43	2·03	1·83	2·03	2·48	1·10			
Mg	3·36	3·05	2·83	2·67	2·44	2·26	3·34			
Mn	0·03	0·02	0·05	0·03	0·04	0·06	0·01			
Ca	1·69	1·76	1·66	1·80	1·77	1·68	1·72			
Na	0·19	0·52	0·32	0·49	0·41	0·30	0·57			
K	0·07	0·09	0·10	0·08	0·09	0·05	0·03			
Σ Cations	14·96	15·37	15·07	15·37	15·27	15·22	15·32			
mg-no.	0·68	0·68	0·58	0·59	0·54	0·53	0·75			

Structural formulae calculated on the basis of 13 cations not including Ca, Na, and K. Major element oxides and F in weight percent; trace elements (by INAA) in p.p.m. na = not analyzed.

medium grained and typically hypidiomorphic; compared with the gabbros they are notably richer in biotite, quartz, ilmenite (partially replaced by magnetite), and apatite (commonly acicular). LKS plagioclase is similar in zoning and range of An content (An_{82-25}) to MKS plagioclase, but has systematically lower Or at equal An. The average Or content of 16 LKS analyses (An_{60-36}, $\bar{x}=An_{47\cdot6}$) is 0·8 mol % vs 2·5 mol % for 33 MKS analyses (An_{60-38}, $\bar{x}=An_{49\cdot5}$). Augite ($Wo_{44}En_{47}Fs_9$–$Wo_{42}En_{36}Fs_{21}$) and hypersthene ($Wo_3En_{65}Fs_{32}$–$Wo_2En_{50}Fs_{47}$) are present at Copper Lake mostly as relict patches in amphibole, except in samples collected near the pluton margins, where amphibole is less abundant. The augites contain $<1\cdot1$ wt % Al_2O_3, consistent with textural evidence that they crystallized at low pressure after pluton emplacement (Table 2, Nos 5–7). Amphibole occurs in the gabbroic unit at Copper Lake as oikocrysts of titaniferous tschermakitic hornblende (Table 3, No. 4), similar to those at Mt Sefrit. Some diorites at Copper Lake also contain intercumulus amphiboles with high Ti and Al, but these have lower *mg*-numbers and Na than the gabbro oikocrysts (Table 3, No. 5). Quartz diorites at Copper Lake contain magnesio- or ferro-hornblende, with lower Ti, Al, and K (Table 3, No. 6; Fig. 2). In general, LKS amphiboles from Copper Lake have higher Al, Ti, and Na/K than MKS amphiboles (excluding the oikocrysts) (Table 3; Fig. 2). Temperatures calculated with amphibole–plagioclase pairs from Copper Lake (Table 1) are >50°C higher than those obtained on MKS samples from Mt Sefrit. Earlier crystallization of amphibole and its higher modal abundance suggest that the differentiated magmas at Copper Lake were richer in water than those at Mt Sefrit. This does not imply that higher water contents are a general feature of LKS magmas relative to MKS magmas. Trace element data (see below) suggest that elevated water contents in dioritic and quartz dioritic magmas at Copper Lake may reflect greater degrees of fractional crystallization rather than higher parent magma water contents. Furthermore, amphibole in the gabbro at Copper Lake, although abundant, is late formed, and LKS plutons elsewhere in the Chilliwack are dominantly pyroxene bearing. In general, primitive LKS magmas probably had lower water contents than their MKS counterparts, based on the lack of phenocrysts in LKS dikes and chilled pluton margins, and on their chemical similarities to tholeiitic basalts elsewhere in the Cascades for which low water contents are indicated by experimental and glass inclusion studies (Sisson & Grove, 1993; Sisson & Layne, 1993).

Several LKS stocks near Whatcom Pass contain tschermakite in hornblendite xenoliths and/or as embayed xenocrysts in fine-grained gabbronorite. The xenocrysts range up to 5 cm in length and are associated with aluminous augites (Table 2, No. 1) similar to those at Mt Sefrit. Relative to other amphiboles, the tschermakites have higher *mg*-numbers, higher Al and Na, and lower K (Table 3, No. 7; Fig. 2). Amphiboles of similar composition have been reported from lower-crustal island arc xenoliths (Aoki, 1971) and from 5-kbar melting experiments on natural basalts (Helz, 1976). The Chilliwack tschermakite xenocrysts, along with the aluminous augites and calcic plagioclase cores, may represent an assemblage of xenocrysts that crystallized from hydrous basaltic magmas at middle- to lower-crustal depths.

CHEMICAL AND Sr–Nd ISOTOPIC COMPOSITIONS

Twenty-seven samples of mafic plutons and one sample of Darrington Phyllite were selected for whole-rock major and trace element analysis (Table 4); Sr and Nd isotope compositions were measured on a subset of 14 samples (Table 5). Analytical methods are given in Appendix A. The samples include specimens from 6 of 11 mafic stocks in the Chilliwack, and were chosen to represent the range of mafic rock types present in the batholith.

Medium-K series

The MKS is calc-alkaline (Fig. 3a,b), and most samples plot in the medium-K field (Fig. 3c). The 11 analyzed samples (olivine gabbronorite to biotite–hornblende quartz diorite) have 51–60 wt % SiO_2 and *mg*-numbers of 70–43. All are high in Al_2O_3 (16·4–23·5 wt %) and contain between 0·3 and 2·4 wt % K_2O. Accumulated pyroxene and/or plagioclase is evident in samples with *mg*-numbers >60, Al_2O_3 >18·5 wt %, or K_2O <0·5 wt %, and probably accounts for much of the scatter on MKS variation diagrams. Sr contents of these rocks are moderately high (780–420 p.p.m.) and correlate inversely with SiO_2. Cr (218–13 p.p.m.) and Ni (163–12 p.p.m.) also decrease with increasing SiO_2 but do not reach the extreme depletions observed in LKS diorites. MKS samples are variably LREE enriched ($La/Yb_N=1\cdot6$–$8\cdot6$). However, all samples from an individual stock have similar La/Yb_N, although with increasing SiO_2 absolute REE contents generally rise and Eu/Eu* values decrease (Fig. 4).

Initial $^{87}Sr/^{86}Sr$ ratios of MKS samples range from 0·70343 to 0·70410 and $\varepsilon_{Nd(0)}$ values vary from +5·3 to +3·5 (Table 5). There is a general correlation

Table 4: Whole rock major and trace element, and modal data

Sample:	82-046	82-106	83-005	88-050	82-048	82-104	87-079
Map unit:	Mt Sefrit (M)	Mt Sefrit (M)	Mt Sefrit (M)	Mt Sefrit (M)	Mt Sefrit (M)	Mt Sefrit (M)	Pass Lake (M)
Rock type:	gab-nor	gab-nor	px diorite	hb diorite	qtz diorite	qtz diorite	px diorite
Analysis:	1,4	1,4	1	1,4	1,4	1,4	3,5
SiO_2	53·10	53·03	54·24	51·25	56·87	59·69	52·72
TiO_2	0·74	0·77	0·63	0·79	0·71	0·83	0·97
Al_2O_3	17·52	16·42	23·49	20·43	18·45	17·27	19·16
Fe_2O_3[a]	1·10	1·83	1·27	7·75	1·94	1·90	1·18
FeO	6·15	6·99	2·61	—	3·99	4·22	5·90
MgO	7·26	7·61	2·15	4·19	3·40	2·53	5·23
MnO	0·13	0·13	0·05	0·11	0·11	0·11	0·14
CaO	9·55	7·94	9·93	10·15	6·42	5·77	8·61
Na_2O	3·12	3·51	3·96	3·35	4·45	4·55	4·06
K_2O	0·93	1·05	1·09	0·98	2·07	1·44	0·71
P_2O_5	0·27	0·31	0·22	0·20	0·27	0·26	0·31
LOI[b]	0·70	0·71	0·41	0·84	1·54	0·92	0·87
Total	100·58	100·29	100·05	100·04	100·22	99·49	99·85
mg-no.	0·64	0·61	0·51	0·52	0·51	0·43	0·57
Ni	59	163	—	15	37	12	36
Cr	164	218	—	60	34	13	56
Sc	28	23	—	23	16	17	22
V	223	184	—	214	143	168	211
Sr	772	476	921[6]	761	526	531	699
Ba	294	472	—	306	606	603	345
Rb	11·9[6]	—	20·7[6]	—	—	44·2[6]	11·2[6]
Cs	0·60[7]	—	—	—	—	—	1·89[7]
U	0·7[7]	—	—	—	—	—	0·7
Th	1·8[7]	—	—	—	—	—	1·9
Pb	5·9[8]	—	—	—	—	—	6·0
Co	53	58	—	49	41	40	24
Zn	72	84	—	57	71	73	90
Cu	49	19	—	21	56	23	15
Nb	3·0[8]	—	—	—	—	—	4·2
Ta	0·15[7]	—	—	—	—	—	0·18
Y	16·5	20·1	—	18·6	22·1	22·5	14·2
Zr	72[8]	37	—	76	167	53	58
Hf	2·2[7]	—	—	—	—	—	1·4
Be	1·1	1·2	—	1·1	2·0	1·7	1·0[4]
Li	13·3	17·7	—	12·2	24·8	19·8	8·4[4]
La	12·1	15·4	—	11·8	14·5	17·9	14·5
Ce	26·5	31·1	—	32·5	30·4	36·8	28·5
Pr	—	—	—	—	—	—	3·7
Nd	14·6	15·4	—	15·4	14·9	17·2	15·2
Sm	3·51	3·73	—	3·46	3·75	4·17	3·28
Eu	1·11	1·02	—	0·99	1·06	1·19	1·24
Gd	3·23	3·62	—	3·01	3·63	3·90	3·17
Tb	—	—	—	—	—	—	0·46
Dy	2·86	3·33	—	3·00	3·53	3·76	2·68
Ho	0·53	0·65	—	0·61	0·70	0·74	0·52
Er	—	—	—	—	—	—	1·55
Tm	—	—	—	—	—	—	0·20
Yb	1·40	1·74	—	1·58	2·02	1·94	1·35
Lu	0·21	0·26	—	0·25	0·31	0·28	0·19

Table 4: Continued

Sample:	82-046	82-106	83-005	88-050	82-048	82-104	87-079
Map unit:	Mt Sefrit (M)	Mt Sefrit (M)	Mt Sefrit (M)	Mt Sefrit (M)	Mt Sefrit (M)	Mt Sefrit (M)	Pass Lake (M)
Rock type:	gab-nor	gab-nor	px diorite	hb diorite	qtz diorite	qtz diorite	px diorite
Analysis:	1,4	1,4	1	1,4	1,4	1,4	3,5
Modes							
Plagioclase	54·2	53·6	81·6	63·2	61·4	64·3	70·8
Olivine	1·6	2·8	—	—	—	—	—
Clinopyroxene	14·9	10·7	7·0	—	0·4	0·4	11·2
Orthopyroxene	21·9	16·9	3·2	—	—	—	7·8
Amphibole	0·4	2·8	—	26·6	14·4[c]	11·6	4·0[c]
Biotite	2·7	6·5	2·4	0·6	11·1	9·1	0·4
Opaque	1·9	1·7	0·6	2·2	1·1	1·6	5·4
Quartz	—	3·3	3·6	3·4	10·3	10·8	—
Orthoclase	2·3	tr	0·8	1·6	—	1·2	—
Other	a,z	a	a	a,z,s,e,c	a,z,s,e,c	a,z,s,e	a

Sample:	87-082	87-060	87-061	89-002	87-026	87-029	87-031
Map unit:	Pass Lake (M)	Peak 6861 (M)	Peak 6861 (M)	Thompson (M)	Whatcom (L)	Whatcom (L)	Whatcom (L)
Rock type:	px diorite	gab-nor	gab-nor	px diorite	px gabbro	px diorite	px diorite
Analysis:	2,5	1,5	2,5	2,5	2,5	3,5	3,5
SiO_2	57·45	57·68	51·76	56·72	55·31	53·94	57·88
TiO_2	0·90	0·55	0·25	0·86	0·62	0·68	0·64
Al_2O_3	17·08	18·42	17·00	17·50	17·99	19·79	18·40
Fe_2O_3[a]	0·61	1·40	0·19	0·14	2·04	7·81	7·24
FeO	5·39	4·71	7·46	6·40	4·91	—	—
MgO	4·13	4·25	9·76	4·10	5·31	4·41	4·52
MnO	0·11	0·12	0·20	0·12	0·17	0·13	0·13
CaO	6·98	7·56	9·72	7·16	7·96	8·99	8·35
Na_2O	3·64	3·46	1·77	3·78	3·01	3·50	3·38
K_2O	2·40	1·22	0·28	1·22	0·47	0·44	0·49
P_2O_5	0·23	0·15	0·03	0·20	0·15	0·15	0·15
LOI[b]	1·04	0·63	1·49	1·72	1·78	0·84	0·78
Total	99·96	100·15	99·89	99·92	99·71	100·67	101·96
mg-no.	0·55	0·56	0·70	0·53	0·58	0·53	0·55
Ni	43	22	36	29	21	20	20
Cr	76	21	77	40	81	11	35
Sc	—	20	32	19	24	26	28
V	144	178	98	167	151	215	188
Sr	632	427	402	407	480	583	575
Ba	647	338	128	324	215	214	283
Rb	55·0	32·3[6]	10·0	33·3	11·7	9·2	8·1
Cs	—	—	2·85	2·28	0·73	0·85	1·02
U	3·9	1·2	0·4	1·4	0·4	0·1	0·2
Th	11·1	2·6	0·8	2·3	0·5	0·1	0·4
Pb	14·1	7·0	5·0	5·4	8·1	5·7	5·5
Co	46	20	50	38	36	48	45

(continued on next page)

Table 4: Continued

Sample:	87-082	87-060	87-061	89-002	87-026	87-029	87-031
Map unit:	Pass Lake (M)	Peak 6861 (M)	Peak 6861 (M)	Thompson (M)	Whatcom (L)	Whatcom (L)	Whatcom (L)
Rock type:	px diorite	gab-nor	gab-nor	px diorite	px gabbro	px diorite	px diorite
Analysis:	2,5	1,5	2,5	2,5	2,5	3,5	3,5
Zn	—	70[4]	—	—	—	—	—
Cu	85	52	14	—	—	—	—
Nb	10·3	4·6	1·2	4·8	3·0	2·2	2·9
Ta	0·61	0·31	0·10	0·15	0·13		
Y	21·5	16·9	11·9	22·3	13·0	13·9	15·6
Zr	220	95	23	158	55		
Hf	5·2	2·7	0·7	4·7	1·9	0·7	0·7
Be	—	0·8[4]	—	—	—	—	—
Li	—	14·6[4]	—	—	—	—	—
La	27·0	8·8	3·3	10·8	5·5	5·1	6·2
Ce	54·5	19·9	7·6	24·8	12·6	11·7	14·1
Pr	6·5	2·6	1·1	3·5	1·8	1·7	2·0
Nd	26·0	11·1	5·0	15·3	8·2	7·7	9·1
Sm	5·16	2·70	1·36	3·64	2·05	1·98	2·25
Eu	1·22	0·76	0·48	1·02	0·74	0·84	0·83
Gd	4·69	2·82	1·54	3·89	2·25	2·21	2·44
Tb	0·65	0·45	0·27	0·62	0·36	0·36	0·40
Dy	3·77	2·81	1·90	3·92	2·36	2·38	2·67
Ho	0·79	0·60	0·43	0·83	0·51	0·51	0·56
Er	2·23	1·72	1·28	2·31	1·45	1·45	1·60
Tm	0·32	0·28	0·22	0·35	0·22	0·22	0·24
Yb	2·12	1·80	1·44	2·24	1·36	1·38	1·56
Lu	0·32	0·27	0·23	0·34	0·21	0·21	0·24
Modes							
Plagioclase	70·2	75·2	53·2		56·6		68·8
Olivine	—	—	—		—		—
Clinopyroxene	12·4	8·2	11·6		2·0		1·6
Orthopyroxene	5·2	7·0	17·0		4·4		2·0
Amphibole	5·4[c]	0·6	16·8[c]		28·6[c]		17·8[c]
Biotite	1·4	4·8	0·2				3·2
Opaque	3·4	4·4	0·4		6·8		3·0
Quartz	2·0	—	0·8		0·4		3·4
Orthoclase	—	—	—		—		—
Other	a		a		a		a,z

(continued on next page)

between $^{87}Sr/^{86}Sr_i$ and degree of differentiation, suggesting that isotopic variation is due at least in part to crustal contamination.

Low-K Series

LKS gabbros and diorites are characterized by high Al_2O_3 (17·3–23·0 wt %) and CaO (6·4–11·3 wt %), low K_2O (0·22–0·74 wt %), and generally low SiO_2 (most <56 wt %). The *mg*-numbers decrease from 65–58 in the gabbros to 55–37 in the diorites. The samples with the highest CaO and Al_2O_3 (87-029, 87-108, 88-022, 88-032) may have accumulated plagioclase. Most LKS samples classify as low-K (Fig. 3c), and the more evolved samples plot in the tholeiitic field on an FeO^*/MgO vs SiO_2 diagram (Fig.

Table 4: Continued

Sample:	87-032	87-108	88-022	88-032	88-025	88-034	88-023
Map unit:	Whatcom (L)	Copper Lake (L)	Copper Lake (L)	Copper Lake (L)	Copper Lake (L)	Copper Lake (L)	Copper Lake (L)
Rock type:	hb qtz dior	hb gabbro	hb gabbro	hb gabbro	hb gabbro	pegmatite	hb diorite
Analysis:	3,5	1,5	1,5	3,5	2,5	3,5	3,5
SiO_2	56·32	49·03	50·88	50·62	53·37	63·95	48·56
TiO_2	0·61	0·64	0·94	0·72	0·57	2·35	2·39
Al_2O_3	18·94	22·98	18·10	21·73	17·33	8·97	17·55
Fe_2O_3[a]	7·42	0·89	0·97	0·51	7·92	0·73	4·04
FeO	—	4·69	7·16	5·65	—	7·80	8·89
MgO	4·64	5·62	6·47	5·86	6·87	4·89	4·17
MnO	0·13	0·10	0·16	0·11	0·15	0·19	0·20
CaO	8·07	11·28	10·45	10·78	8·84	7·05	8·08
Na_2O	3·47	3·31	3·79	3·19	2·84	2·58	4·14
K_2O	0·43	0·38	0·32	0·30	0·43	0·22	0·29
P_2O_5	—	0·20	0·22	0·10	0·13	1·18	0·63
LOI[b]	1·06	1·54	1·15	1·65	1·34	1·33	1·26
Total	101·09	100·66	100·61	101·21	99·79	101·25	100·19
mg-no.	0·55	0·65	0·59	0·63	0·63	0·51	0·37
Ni	20	39	28	37	51	15	8
Cr	24	50	107	58	48	23	<1
Sc	28	23	31	23	27	—	—
V	198	124	213	128	197	206	307
Sr	561	581	431	520	469	214	453
Ba	192	123	157	146	196	113	278
Rb	11·3	3·0[6]	3·5[6]	6·1	10·5	1·4	2·2
Cs	0·65	—	0·21	—	—	—	—
U	0·1	0·1	0·1	0·2	0·2	1·3	0·4
Th	0·4	0·2	0·2	0·4	0·2	5·1	0·6
Pb	11·1	2·4	1·2	2·4	5·9	2·7	3·7
Co	40	51	37	42	46	82	45
Zn	—	58[4]	69[4]	—	—	—	—
Cu	—	19	15	19	58	5	11
Nb	2·5	1·9	2·3	2·0	2·5	14·8	7·1
Ta	—	—	0·11[7]	0·13	—	0·88	0·34
Y	13·6	10·9	16·6	11·2	11·8	47·0	25·1
Zr	—	50	66	53	35	284	66
Hf	0·4	1·1	1·8	1·3	1·1	6·8	1·8
Be	—	1·3	1·5	—	—	—	—
Li	—	14·7	13·6	—	—	—	—
La	6·6	3·5	4·6	4·6	4·8	30·4	12·6
Ce	14·4	8·8	12·3	9·8	10·8	68·9	30·5
Pr	2·0	1·2	1·9	1·4	1·5	9·4	4·3
Nd	8·5	5·8	9·1	6·4	6·9	40·4	18·5
Sm	2·04	1·56	2·52	1·67	1·78	8·96	4·65
Eu	0·78	0·62	0·96	0·70	0·67	1·48	1·50
Gd	2·21	1·83	2·92	1·90	1·93	9·20	5·18
Tb	0·36	0·28	0·47	0·28	0·32	1·43	0·74
Dy	2·30	1·94	3·18	2·08	2·11	8·75	4·79
Ho	0·49	0·35	0·65	0·38	0·44	1·79	0·93
Er	1·39	1·06	1·96	1·11	1·28	4·86	2·54
Tm	0·21	0·14	0·27	0·17	0·20	0·73	0·39
Yb	1·30	1·06	1·83	1·12	1·23	4·34	2·36
Lu	0·20	0·13	0·25	0·15	0·19	0·67	0·36

(continued on next page)

Table 4: Continued

Sample:	87-032	87-108	88-022	88-032	88-025	88-034	88-023
Map unit:	Whatcom (L)	Copper Lake (L)	Copper Lake (L)	Copper Lake (L)	Copper Lake (L)	Copper Lake (L)	Copper Lake (L)
Rock type:	hb qtz dior	hb gabbro	hb gabbro	hb gabbro	hb gabbro	pegmatite	hb diorite
Analysis:	3,5	1,5	1,5	3,5	2,5	3,5	3,5
Modes							
Plagioclase	67·9	60·6	53·4	60·6	69·8	18·2	57·4
Olivine	—	—	—	—	—	—	—
Clinopyroxene	—	—	8·0	1·0	1·6	—	1·8
Orthopyroxene	—	—	3·6	—	2·8	—	—
Amphibole	20·2[c]	39·8[c]	34·2	36·6[c]	18·6[c]	45·8	28·5
Biotite	2·2	—	0·2	0·6	—	—	4·1
Opaque	4·0	—	0·6	0·4	5·4	2·4	5·7
Quartz	5·6	—	—	—	—	29·0	0·8
Orthoclase	—	—	—	—	—	—	—
Other	a,z,s,e,c	a,e	a,s	a,s,e,c	a	a	a,s

Sample:	87-107	87-109	88-053	88-055	87-112	83-011	DP-1
Map unit:	Copper Lake (L)	Copper Lake (L)	Copper Lake (L)	Copper Lake (L)	Copper Lake (L)	dike (L)	Darrington
Rock type:	hb diorite	hb diorite	px diorite	hb qtz dior	hb qtz dior	hb diorite	phyllite
Analysis:	3,5	1,4	1,4	2,5	1,4	1,4	1,4
SiO_2	49·11	45·83	51·54	56·54	55·46	48·30	65·27
TiO_2	2·33	2·01	1·76	1·48	1·14	1·06	0·68
Al_2O_3	18·20	17·51	18·42	17·63	17·89	20·09	15·29
Fe_2O_3[a]	1·75	4·25	10·64	1·45	9·23	5·24	5·92
FeO	8·84	9·24	—	6·68	—	4·92	—
MgO	4·67	5·41	3·67	2·70	2·91	4·42	2·80
MnO	0·20	0·19	0·24	0·20	0·20	0·14	0·12
CaO	8·88	9·74	7·88	6·44	6·42	9·13	3·17
Na_2O	3·65	3·41	4·69	4·79	5·43	4·39	2·75
K_2O	0·38	0·27	0·22	0·71	0·71	0·74	1·14
P_2O_5	0·80	0·29	0·83	0·58	0·39	0·38	0·30
LOI[b]	1·25	1·45	-0·08	1·03	0·22	2·05	2·72
Total	100·06	99·60	99·80	100·21	100·00	100·85	100·16
mg-no.	0·44	0·42	0·41	0·38	0·38	0·45	0·48
Ni	3	3	4	1	2	7	67
Cr	3	6	bd	0	bd	bd	154
Sc		40	29	—	19	23	18
V	226	636	143	98	74	265	167
Sr	688	617	723	627	617	589	195
Ba	233	185	293	456	455	239	235
Rb	7·4	1·8[6]	1·2[6]	13·1	12·3[6]	14·1[6]	44·4[6]
Cs	—	0·28[7]	—	—	—	—	—

(continued on next page)

Table 4: Continued

Sample:	87-107	87-109	88-053	88-055	87-112	83-011	DP-1
Map unit:	Copper Lake (L)	Copper Lake (L)	Copper Lake (L)	Copper Lake (L)	Copper Lake (L)	dike (L)	Darrington
Rock type:	hb diorite	hb diorite	px diorite	hb qtz dior	hb qtz dior	hb diorite	phyllite
Analysis:	3,5	1,4	1,4	2,5	1,4	1,4	1,4
U	0·2	0·2[7]	—	0·5	—	—	—
Th	0·4	0·2[7]	—	0·9	—	—	—
Pb	2·3	3·9[8]	—	4·9	—	—	—
Co	43	37	77	43	32	51	88
Zn	—	94	126	—	108	70	113
Cu	7	22	7	3	4	20	69
Nb	5·6	3·3[5]	11·7	11·1	4·2	3·1	28·1
Ta	0·41	0·14[7]	—	0·59	—	—	—
Y	17·3	26·9	34·9	28·1	36·1	26·0	22·2
Zr	39	33[8]	26	75	17	23	153
Hf	1·0	1·5[5]	—	1·8	—	—	—
Be	—	0·9	0·8	—	1·0	1·1	2·8
Li	—	5·2	7·2	—	17·1	19·0	48·4
La	11·3	7·6	16·2	15·5	18·3	10·5	20·7
Ce	26·3	21·8	38·2	37·8	43·2	30·8	41·2
Pr	3·7	—	—	5·3	—	—	—
Nd	15·4	15·2	25·5	23·4	26·6	17·4	19·1
Sm	3·49	4·45	6·86	5·53	6·73	4·58	3·56
Eu	1·52	1·48	2·35	2·21	2·11	1·47	1·12
Gd	3·72	4·53	6·87	5·89	6·49	4·41	3·26
Tb	0·52	—	—	0·85	—	—	—
Dy	3·12	4·85	5·87	5·01	5·87	4·58	2·63
Ho	0·62	0·96	1·21	1·05	1·26	0·87	0·50
Er	1·61	—	—	2·89	—	—	—
Tm	0·23	—	—	0·39	—	—	—
Yb	1·45	2·27	2·28	2·43	2·63	2·26	1·34
Lu	0·21	0·34	0·33	0·34	0·39	0·34	0·18
Modes							
Plagioclase	65·2	55·4		63·0	68·2	67·2	
Olivine	—	—		—	—	—	
Clinopyroxene	0·8	1·7		0·7	—	—	
Orthopyroxene	—	—		—	—	—	
Amphibole	23·8[c]	35·9		24·0	18·9	25·0	
Biotite	3·0	0·5		3·6	5·8	0·6	
Opaque	4·2	5·3		2·0	2·2	4·8	
Quartz	1·0	—		5·3	4·4	—	
Orthoclase	—	—		—	—	—	
Other	a	a		a,z	a,al	a,s,e	

Major oxides in weight percent; trace elements in parts per million. Map unit includes (M) for medium-K series, (L) for low-K series. Rock type abbreviations: gab-nor, gabbronorite; px, pyroxene; hb, hornblende; qtz, quartz. Analytical methods: [1]major elements by ICP-ES; [2]major elements by XRF; [3]major elements by DCP-ES; [4]trace elements by ICP-ES; [5]trace elements by ICP-MS; [6]Rb or Sr by isotope dilution; [7]trace element by INAA; [8]trace element by XRF. [a]In samples for which FeO was not determined, total Fe is reported as Fe_2O_3. [b]LOI (loss on ignition) values have been adjusted to remove weight gain owing to oxidation of FeO in samples where FeO is reported. Modes determined by point count (500–1000 points); tr, trace amounts. [c]Total includes secondary amphibole after pyroxene; 'Other' minerals are apatite (a), allanite (al), zircon (z), sphene (s), epidote (e), chlorite (c).

Table 5: Whole-rock isotopic data

Sample no.	Age (Ma)	Rb (p.p.m.)	Sr (p.p.m.)	$^{87}Rb/^{86}Sr$	$^{87}Sr/^{86}Sr$	$^{87}Sr/^{86}Sr_i$	$^{143}Nd/^{144}Nd$	$\varepsilon_{Nd(0)}$
Medium-K series								
82-046	22·9±0·1	11·9	772·4	0·0443	0·703439	0·703424	0·512883	+4·84
82-104	22·9±0·1	44·2	531·1	0·2395	0·703935	0·703857	0·512865	+4·49
83-005	22·9±0·1	20·7	920·8	0·0647	0·704045	0·704024	0·512814	+3·49
87-060	18±17[a]	32·3	416·5	0·2232	0·704153	0·704096	0·512865	+4·49
87-079	23±12[a]	11·2	676·7	0·0476	0·703754	0·703738	0·512906	+5·29
88-038	22·9±0·1	16·8	693·3	0·0697	0·703816	0·703793		
Low-K series								
83-011	18±17[a]	14·1	588·7	0·0689	0·703851	0·703833	0·512880	+4·78
87-108	34·0±0·9	3·0	570·9	0·0151	0·703548	0·703540	0·512989	+6·91
87-109	34·0±0·9	1·8	616·6	0·0084	0·703809	0·703804	0·512899	+5·15
87-112	34·0±0·9	12·3	616·8	0·0574	0·703866	0·703835	0·512884	+4·86
88-022	34·0±0·9	3·5	457·7	0·0220	0·703451	0·703439	0·512946	+6·07
88-053	34·9±0·9	1·2	723·2	0·0048	0·703838	0·703835	0·512900	+5·17
88-023	34·9±0·9	4·7	530·0	0·0254	0·703803	0·703789		
Darrington Phyllite								
DP-1		44·4	195·4	0·6544	0·709198	0·709031[b]	0·512469	−3·24

Analytical uncertainties for Rb and Sr concentrations are 0·1% and 5%, respectively. Sr isotope ratios normalized to $^{86}Sr/^{88}Sr = 0·1194$; analytical uncertainty (2σ) is 0·000040 based on 41 analyses of NBS987 with an average measured $^{87}Sr/^{86}Sr = 0·71026$. Nd isotope ratios were normalized to $^{146}Nd/^{144}Nd = 0·7219$ and have 2σ analytical uncertainty of 0·000024, based on 36 analyses of La Jolla Nd with an average measured $^{143}Nd/^{144}Nd = 0·511849$. $\varepsilon_{Nd(0)}$ values were calculated relative to 0·512635. Measured $^{143}Nd/^{144}Nd$ are within analytical error of initial ratios owing to the young age of the Chilliwack plutons. [a]For undated plutons an age of 18±17 Ma is assumed unless field relations provide tighter constraints. [b]Initial ratio calculated for time of intrusion by Mt Sefrit pluton (22·9 Ma).

3b). However, high Al_2O_3 and Na_2O contents place most samples within the calc-alkaline fields on AFM (Fig. 3a) and Al_2O_3 vs normative plagioclase diagrams (Irvine & Baragar, 1971).

All LKS samples (excluding pegmatite 88-034) are low in incompatible trace elements, notably Rb (1–14 p.p.m.) and Th (<1 p.p.m.). The gabbros have relatively unfractionated REE ($La/Yb_N = 1·7–2·7$) and positive Eu anomalies (Fig. 4d,e), whereas the diorites have higher and more variable La/Yb_N (2·3–5·3) (Fig. 4d,f). Among samples from Copper Lake, Sr contents increase with fractionation index (430–720 p.p.m.), whereas Cr and Ni contents decrease markedly (110–50 and 50–30 p.p.m., respectively, in the gabbros; <10 p.p.m. each in the diorites).

Isotopic ratios for the LKS gabbros are $^{87}Sr/^{86}Sr_i = 0·70344–0·70354$ and $\varepsilon_{Nd(0)} = +6·1$ to +6·9, whereas the four diorites cluster tightly between $^{87}Sr/^{86}Sr_i = 0·70379–0·70384$ and $\varepsilon_{Nd(0)} = +4·8$ to +5·2 (Table 5). Rb/Sr ratios of all LKS samples are too low to produce the measured $^{87}Sr/^{86}Sr$ values within the age of the Earth, probably indicating some Rb loss. Rb mobility is also suggested by low levels in pegmatite 88-034, which is interpreted as a late differentiate, and contains high levels of immobile incompatible elements (Th, Nb, La) (Table 4).

COMPARISON OF MKS, LKS, AND CASCADE ARC VOLCANIC ROCKS

Major and trace element characteristics of MKS and LKS gabbros suggest that they are the intrusive counterparts of calc-alkaline basalts and basaltic andesites (CAB) and low-K olivine tholeiites (LKOT) found elsewhere in the Cascades. MKS and LKS gabbros are less primitive than most Cascade basalts, but compositional differences between the two series closely parallel the differences between CAB and LKOT (Table 6). In particular, the LKS–LKOT differs from the MKS–CAB in having lower SiO_2, Na_2O and K_2O, and higher CaO and Na_2O/K_2O (Fig. 3d). The high CaO (and Al_2O_3) contents

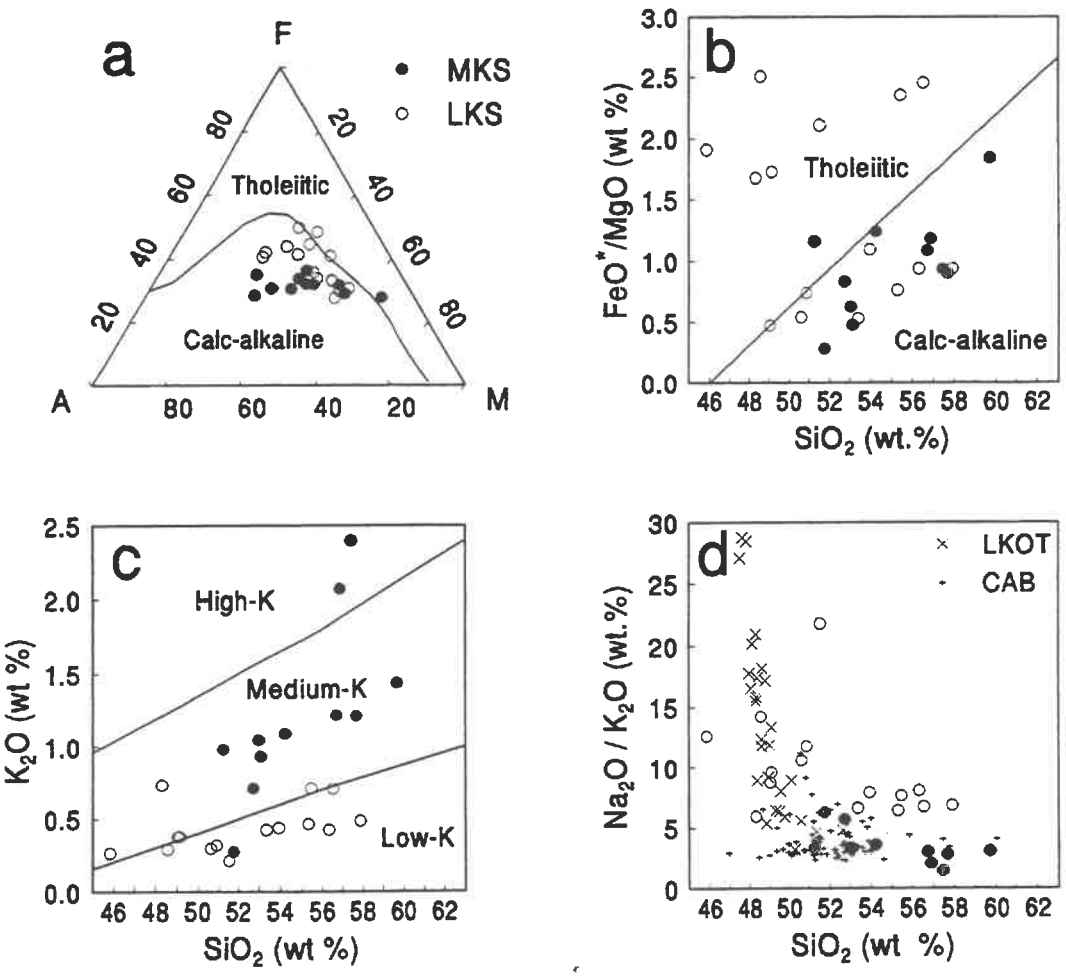

Fig. 3. Classification of mafic pluton samples according to selected major element characteristics. (a) AFM diagram with discrimination line of Irvine & Baragar (1971). (b) FeO*/MgO diagram with discriminant line of Miyashiro (1974). (c) K_2O vs SiO_2 diagram with field boundaries from Rickwood (1989). (d) Na_2O/K_2O vs SiO_2 plot comparing Chilliwack samples with Miocene–Recent low-K olivine tholeiites (LKOT) and calc-alkaline basalts and basaltic andesites (CAB). Data for volcanic rocks in (d) compiled from Bacon (1990), Hughes (1990), Leeman *et al.* (1990), and Clynne (1993).

of some LKS samples could be due in part to plagioclase accumulation, but this process cannot account for contrasts in Na_2O/K_2O because >50% plagioclase addition would be required to produce the observed differences. Similarly, plagioclase accumulation and/or loss of intercumulus melt are not responsible for the low K_2O contents of the LKS. Lower K_2O contents of LKS melts are reflected in mineral compositions (lower Or contents in plagioclase; higher Na/K in amphibole), and the average K_2O content of Copper Lake gabbro (0·38 wt %) agrees closely with the melt composition calculated from plagioclase core K_2O contents (0·40 wt % assuming $D = 0{\cdot}20$; Phinney & Morrison, 1990).

The similarities between MKS gabbros and CAB, and between LKS gabbros and LKOT, are further illustrated by comparison of their trace element and isotopic characteristics. Trace element distinctions of LKOT relative to CAB include lower abundances of most incompatible elements (particularly Rb, Ba, Sr, LREE, Th), lower $(La/Yb)_N$, and higher HREE and Sc (Table 6). These same distinctions are observed in comparing LKS and MKS gabbros (Table 6, Fig. 5a), although LKS gabbros do not have lower HREE contents until adjustments are made to account for plagioclase loss or accumulation (see next section). On mantle-normalized trace element diagrams (Fig. 5) MKS and LKS gabbros show large-ion lithophile element (LILE) enrichments (Rb, K, Sr, Ba, U) and high field strength element (HFSE) depletions (Nb, Ta) characteristic of arc magmas, and their trace element patterns generally overlap with those of the volcanic rocks. Initial Sr and Nd isotopic compositions of Chilliwack gabbros

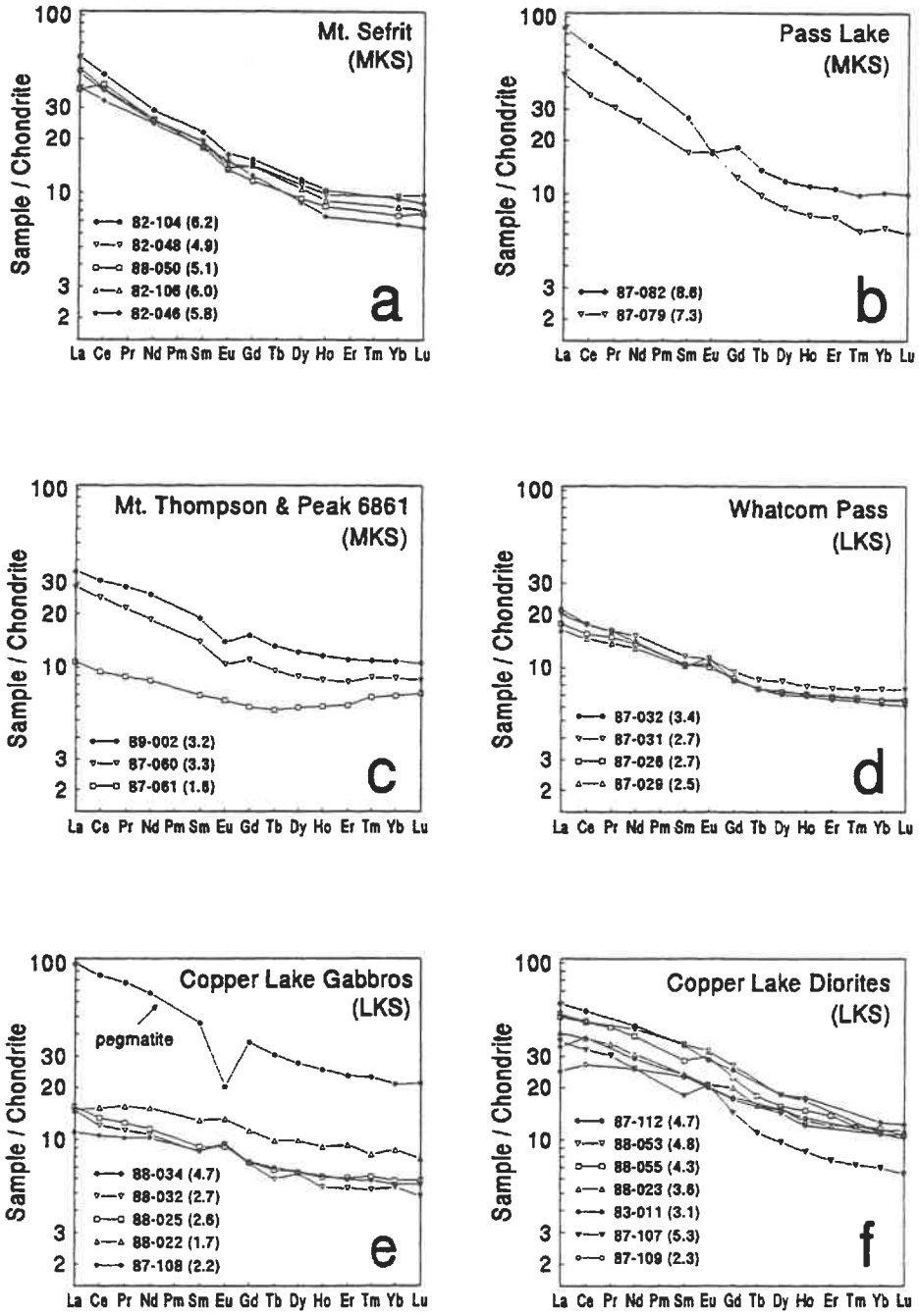

Fig. 4. REE data for Chilliwack gabbros and diorites, normalized to the recommended chondrite values of Boynton (1984). La/Yb_N for each sample is given in parentheses.

lie within the range of Cascade lavas (Fig. 6). There is no pronounced difference in $^{87}Sr/^{86}Sr_i$ between LKS and MKS samples; however, LKS gabbros have notably higher $\varepsilon_{Nd(0)}$. A similar distinction is recognized in the Lassen Peak area, where LKOT differ from CAB in having higher $\varepsilon_{Nd(0)}$ at equal $^{87}Sr/^{86}Sr_i$ (M. Clynne, personal communication, 1993).

INVERSE REE MODELING AND SOURCE CHARACTERISTICS

The four least-differentiated MKS gabbros (82-046, 87-060, 87-079, 87-082) are from three different plutons, but have similar incompatible element ratios (variation $<2\sigma$ analytical uncertainty) and

Table 6: Comparison of MKS and LKS gabbros with Cascade basalts

	MKS (5)		LKS (5)		CAB (68)		LKOT (28)	
SiO_2	54·80	(2·26)	51·84	(2·22)	52·02	(2·11)	49·01	(1·14)
TiO_2	0·79	(0·14)	0·70	(0·13)	1·24	(0·37)	1·14	(0·28)
Al_2O_3	17·72	(0·97)	19·63	(2·28)	17·12	(0·76)	17·45	(0·46)
FeO(t)	6·93	(0·99)	6·70	(0·87)	8·24	(1·09)	9·48	(0·60)
MgO	5·70	(1·47)	6·03	(0·57)	7·19	(1·52)	8·63	(1·39)
CaO	8·13	(0·89)	9·86	(1·25)	8·99	(0·98)	10·51	(0·97)
Na_2O	3·56	(0·30)	3·23	(0·32)	3·52	(0·45)	2·94	(0·36)
K_2O	1·26	(0·59)	0·38	(0·06)	1·00	(0·34)	0·33	(0·25)
P_2O_5	0·25	(0·06)	0·16	(0·05)	0·32	(0·15)	0·16	(0·08)
Na/K	3·35	(1·35)	8·90	(2·14)	4·00	(1·62)	13·25	(7·25)
mg-no.	0·59	(0·03)	0·62	(0·02)	0·60	(0·05)	0·61	(0·05)
Ni	64	(51)	36	(11)	118	(45)	153	(40)
Cr	107	(73)	68	(23)	233	(114)	254	(77)
Sc	23	(3)	26	(7)	25	(5)	34	(3)
Sr	595	(131)	497	(51)	615	(222)	297	(74)
Ba	414	(132)	167	(33)	357	(121)	164	(127)
Rb	27·6	(17·9)	7·0	(3·6)	17·2	(7·3)	4·6	(3·0)
Th	4·3	(3·9)	0·3	(0·1)	2·0	(1·1)	0·9	(0·6)
Y	18·7	(2·1)	12·8	(2·0)	22·8	(4·4)	26·1	(3·2)
La	15·6	(6·2)	4·6	(0·7)	16·4	(8·3)	8·0	(5·5)
Yb	1·7	(0·3)	1·3	(0·3)	2·0	(0·3)	2·6	(0·3)
$(La/Yb)_N$	6·2	(1·8)	2·4	(0·4)	5·8	(3·2)	2·2	(1·6)

Major oxides in weight percent; trace elements in parts per million. Reported values are averages (1 SD in parentheses); number of samples of each rock type given in parentheses in column heading. Data for volcanic rocks from Bacon (1990), Hughes (1990), Leeman *et al.* (1990), and Clynne (1993).

initial Sr and Nd isotopic compositions. However, they display considerable variation in La/Yb_N (3·3–8·6) and incompatible element abundances (e.g. 294–647 p.p.m. Ba). This variation is not attributable to fractionation and/or contamination of a common parental magma type because the samples have overlapping *mg*-numbers and transition metal contents. On plots of C^H/C^i vs C^H (where H is a highly incompatible element and i is moderately to highly incompatible) these gabbros define linear arrays, consistent with their derivation from similar sources by different degrees of melting (Minster & Allègre, 1978). To investigate this hypothesis and constrain the trace element and mineralogical characteristics of the source(s), the REE have been modeled using an inverse technique (Hofmann & Feigenson, 1983). In this method, data for a suite of samples, assumed to represent primary magmas formed by batch partial melting, are plotted on C^{REF}/C^i vs C^{REF} diagrams, where C^{REF} is the concentration of a highly incompatible reference element (in this case La). For each element i, linear regression yields a slope S^i and intercept I^i, which are functions of initial source bulk distribution coefficient D_0^i, initial source concentration C_0^i, and P^i, the bulk distribution coefficient weighted according to the proportions in which the phases involved contribute to the melt:

$$I^i = (C^{La}/C_0^i)\ (1-P^i) \qquad (1)$$

and

$$S^i = D_0^i/C_0^i\ . \qquad (2)$$

Equation (1) can be rearranged to obtain C_0^i relative to an arbitrary source concentration of La:

$$C_0^i/C_0^{La} = (1-P^i)/I^i. \qquad (3)$$

Similarly, equations (2) and (3) can be combined to obtain D_0^i relative to C_0^{La}:

$$D_0^i/C_0^{La} = (S^i/I^i)\ (1-P^i). \qquad (4)$$

None of the MKS gabbros represent primary magmas, so before the data can be inverted the trace element concentrations must be adjusted for the

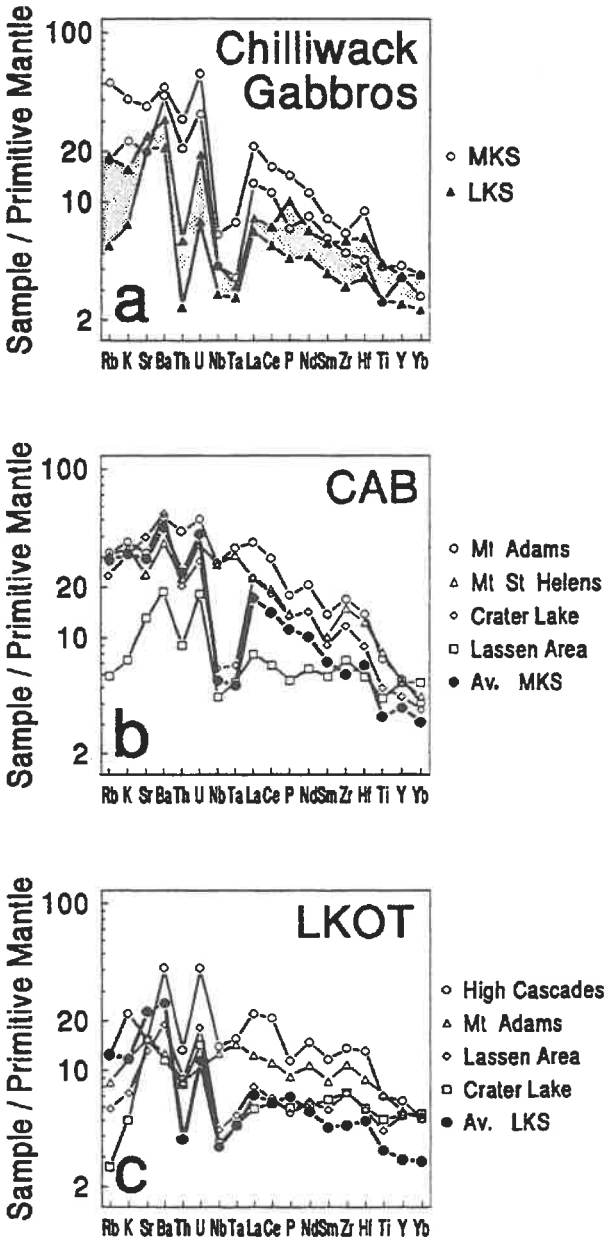

Fig. 5. Trace element abundance diagrams, normalized to the primitive mantle values of Sun & McDonough (1989). (a) Comparison of fields for MKS (five samples) and LKS (five samples) gabbros. It should be noted that although elemental abundances are lower in the LKS, both series display LILE enrichment (e.g. Ba, U) and relative depletions in HFSE (Nb, Ta). (b) Comparison of average MKS gabbro with average CAB from selected Cascade volcanic centers. (c) Comparison of average LKS gabbro with average LKOT from selected Cascade volcanic centers. Data for CAB and LKOT from sources listed in Fig. 3.

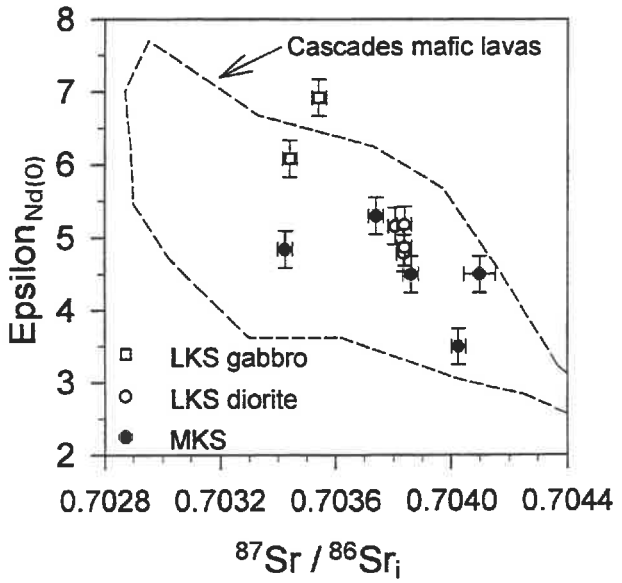

Fig. 6. Initial Sr isotopic composition and $\varepsilon_{Nd(0)}$ of 11 MKS and LKS samples. (Note the higher $\varepsilon_{Nd(0)}$ of the LKS gabbros relative to other Chilliwack samples.) Dashed line outlines the field of 58 Quaternary Cascade mafic lavas compiled from Halliday *et al.* (1983), Grove *et al.* (1988), Leeman *et al.* (1990), and T. Bullen (unpublished data, 1993).

effects of fractional crystallization. Because neither the exact proportions of phases crystallized nor the exact compositions of the primary magmas are known, the samples have been adjusted assuming that only olivine and plagioclase have been removed. The amount of olivine lost was estimated by adding olivine to each sample in 0·5 wt % increments until it reached Fe/Mg equilibrium with representative mantle olivine (Fo_{92}). Assuming $K_{(Fe/Mg)}^{(ol/liq)} = 0{\cdot}324$ [calculated for 10 kbar after Ulmer (1989)] and $Fe^{2+}/(Fe^{2+}+Fe^{3+})_{magma} = 0{\cdot}9$, calculated olivine losses for the four gabbros ranged from 18 to 25 wt %. Plagioclase loss was determined on the basis of the amount required to remove the observed Eu anomalies [assuming $D_{Eu} - D_{Eu^*} = 0{\cdot}75$; calculated for quartz–fayalite–magnetite (QFM) from McKay (1989)], and ranged from 0 to 32%, except in 87-79, for which Eu/Eu* = 1·16 indicated ~22% plagioclase accumulation. Using the Rayleigh equation and distribution coefficients from Appendix B to adjust for these olivine ± plagioclase losses (or accumulation), REE contents of the four MKS gabbros are lowered by 5–38%, but the average change in La/Yb_N is <2%. This fractionation adjustment cannot be utilized for compatible elements (owing to uncertainties in phase proportions and distribution coefficients), and probably ignores loss of clinopyroxene and/or an oxide phase in some samples, but high R^2 values obtained in the subsequent regressions (Table 7) suggest that errors associated with these adjustments do not significantly change the model results as long as the inversion is restricted to the REE.

Table 7: Results of inverse REE modeling

	Slope	Intercept	R^2	C_0	D_0
La	—	—	—	5·00	—
Ce	0·005 (02)	1·06 (04)	0·823	4·28	0·020
Pr	0·008 (00)	1·16 (00)	1·000	3·77	0·032
Nd	0·014 (02)	1·22 (07)	0·942	3·37	0·047
Sm	0·036 (08)	1·21 (21)	0·916	2·73	0·097
Eu	0·053 (13)	1·10 (38)	0·888	2·67	0·143
Gd	0·061 (09)	1·27 (25)	0·958	2·07	0·126
Tb	0·090 (19)	1·13 (52)	0·958	2·13	0·191
Dy	0·114 (14)	0·80 (39)	0·971	2·65	0·302
Ho	0·120 (10)	1·06 (28)	0·986	1·97	0·237
Er	0·128 (17)	0·85 (46)	0·983	2·39	0·306
Yb	0·140 (11)	0·77 (30)	0·989	2·54	0·356
Lu	0·148 (16)	0·81 (45)	0·977	2·42	0·357

Sample	F	olivine	opx	cpx	spinel
Source	—	50·00	20·00	27·00	3·00
87-82	0·09	54·03	20·01	22·89	3·07
87-79	0·13	55·80	20·01	21·08	3·10
82-46	0·16	57·54	20·02	19·31	3·13
87-60	0·27	64·82	20·04	11·88	3·26

Slope, intercept, and R^2 of regressed line are reported for each element, along with resulting calculated initial source REE (C_0) and initial bulk distribution coefficients (D_0). Numbers in parentheses are standard errors in regressed values, expressed relative to last decimal place. C_0 expressed relative to an arbitrary La_N of five. Also summarized are calculated weight fraction of melt (F), and mineral proportions of residuum (in wt%) required to produce the four modeled samples.

The REE inversion results provide two general constraints on the MKS source, which are independent of the choice of P^i: (1) regressed intercept values (Table 7) show a general increase from Ce to Gd, indicating that the source was LREE enriched. This arises from equation (1) and the requirement that, for any plausible mineral assemblage, P^i values will also increase from Ce to Gd, regardless of melting mode. (2) The positive intercept for Lu requires $P^{Lu}<1$ [see equation (1)], and thereby limits the role of garnet to <12% of the melt (assuming $\overline{D}^{Lu}_{gar}=8$ and ignoring the contribution to P^{Lu} made by clinopyroxene). Neither of these constraints is sensitive to the choice of $\overline{D}$ values used, or to a 25% increase or decrease in the amount of olivine + plagioclase added in the fractionation adjustments. The slope and intercept values obtained by regression were used, along with the spinel lherzolite melting mode of Kelemen *et al.* (1990) and the distribution coefficients in Appendix B, to calculate source REE contents, initial bulk distribution coefficients, and the degree of melting required for each sample (Table 7; Fig. 7). Source REE are reported relative to $La_N=5$, which is an arbitrary value. However, if MKS magmas formed by partial melting in the 5–40% range as commonly accepted for tholeiitic basalts (Jaques & Green, 1980), La_N of the MKS source is constrained to 2–9. HREE contents relative to La in the MKS source are less tightly constrained than the LREE (Fig. 7), primarily because of larger uncertainties associated with the intercept values (which, for HREE, are also more sensitive to the fractionation adjustments). Source D values calculated by REE inversion closely match those for spinel lherzolite (Fig. 7), indicating that no garnet is required in the MKS source. Use of lower D values for clinopyroxene would allow a maximum of ~7% garnet in the melt and ~4% in the source before the discrepancy between model and calculated source D^{Lu} values exceeds 50%. However, this small contribution of garnet to the melt contradicts experimental data (Harrison, 1981), which indicate that garnet should be a major component of a melt produced from garnet lherzolite. In summary, results of this modeling are consistent with derivation of the four least-differentiated MKS gabbros by 9–27% melting of an LREE-enriched source ($La/Yb_N \sim 2$) that contained little or no garnet.

Limited variation in REE content among LKS

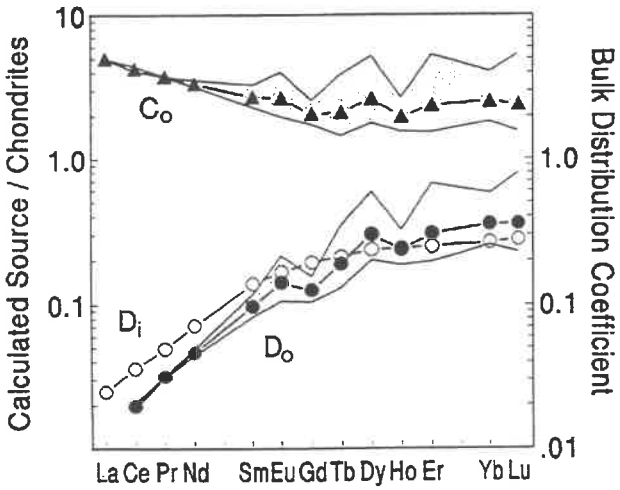

Fig. 7. Chondrite-normalized REE content (C_0) and initial bulk distribution coefficients (D_0) of MKS source as obtained from inverse model. REE contents are expressed relative to an arbitrary La_N content of five. Shaded areas indicate uncertainties based on standard error in regressed slope and intercept values (Table 7). [Note similarity between D_0 and input value (D_i), which was calculated for a source with 50% olivine, 20% opx, 27% cpx, and 3% spinel.]

gabbros (e.g. $La_N = 11–17$) precludes application of the inversion technique to these samples. However, we can still examine the extent to which the LKS source might have been mineralogically and/or chemically different from that of the MKS. After adjustment for 14–21% olivine loss and 12–23% plagioclase accumulation, REE contents of LKS gabbros 87-026 and 88-025 are closely reproduced by 31 and 34% melting of sources with the same REE and mineralogical characteristics as the MKS source. Estimated concentrations of K, Rb, Ba, U, Th, and Nb (calculated with F values from the REE modeling and $P = 0{\cdot}001$) overlap between MKS and LKS sources for all elements except Th, which is lower in the LKS source. There is greater uncertainty associated with these elements owing to possible effects of contamination or mobility (for Rb and Ba) and lower analytical precision (for Th, U, Nb at low levels), but these results are consistent with derivation of MKS and LKS magmas from similar sources, and suggest that lower incompatible element abundances in the LKS could result, at least in part, from derivation at higher degrees of melting. However, differences in incompatible trace element ratios (e.g. La/Th, Hf/Th, U/Nb) indicate that MKS and LKS sources were chemically distinct in terms of some immobile trace elements. In addition, the higher $\varepsilon_{Nd(0)}$ of LKS gabbros suggests that their source had lower Nd/Sm, and that differences in LREE enrichment between LKS and MKS sources were long-standing.

DIFFERENTIATION OF MKS AND LKS MAGMAS

Chemical differences between MKS and LKS plutons reflect not only contrasts inherited from their mantle source regions, but also contrasts in magma evolution. Differentiation of both series was investigated through modeling of major element, trace element, and isotopic data. Major element variation was modeled with the least-squares mixing program PETMIX (K. Laurent, US Geological Survey). Eight oxides were included in these calculations and solutions that yielded reasonable mineral proportions and a squared sum of residuals (ΣR^2) $< 0{\cdot}20$ were considered acceptable. Where there is isotopic evidence of open system differentiation, trace element and isotopic data were modeled using equations for combined assimilation–fractional crystallization (AFC) [equations (6a) and (15b) of DePaolo (1981)]. Closed system differentiation was modeled using the Rayleigh equation for fractional crystallization.

Medium-K series differentiation

The MKS includes a range of rock types from gabbronorite to quartz diorite. All of these lithologies are present within the composite pluton at Mt Sefrit, where field and petrographic data suggest that the various rock types are comagmatic. Evidence of their common parentage includes a close spatial and temporal association, systematic variations in mode and mineral composition, and a progression through time toward more evolved compositions. In addition, all the rocks of this pluton contain plagioclases with the same distinctive zoning. The following discussion focuses on the Mt Sefrit pluton, but the petrologic similarity of other MKS stocks suggests that they record similar magma evolution histories.

Least-squares modeling of major element data for Mt Sefrit rocks (Table 8) is consistent with derivation of these samples from a common parent magma (represented by gabbronorite 82-046) by 19–56% crystallization of plag + olivine + augite + ilmenite, accompanied in some cases by modest crystal accumulation (evident in modal data) and minor apatite removal (required to account for the lack of P_2O_5 enrichment with differentiation). Mineral compositions used in these calculations obviously represent averages over the range of crystallization, but modest changes in these compositions ($An_{61–75}$; $Fo_{66–75}$) have a negligible effect on the results. In contrast, substitution of orthopyroxene for olivine yields consistently higher residuals and leads to higher calculated degrees of crystallization, which conflict with the trace element data.

Modeling of trace element and isotopic variation among Mt Sefrit samples supports the hypothesis that these rocks are related by fractional crystallization, accompanied by wallrock assimilation. The AFC process was modeled using data for the least and most differentiated samples (82-046 and 82-104). Darrington Phyllite (DP-1) was taken to be the assimilant because xenoliths of Darrington Phyllite hornfels occur in varying stages of digestion throughout the Mt Sefrit pluton. The minerals removed during crystallization and their proportions were obtained from the PETMIX results (Table 8), along with 0·7% apatite. With 50–55% crystallization, distribution coefficients from Appendix B, and a mass assimilated/mass crystallized ratio (M_a/M_c) of 0·25–0·30, results of the AFC calculations closely match observed values in 82-104 for Rb, Sr, Ba, Cr, Sc, Ni and $^{87}Sr/^{86}Sr$. However, calculated REE abundances are 20–60% too high and calculated ε_{Nd} values are 1·3 epsilon units too low. Increasing the amount of apatite removed improves the REE results, but exacerbates the ε_{Nd} mismatch.

Table 8: Least-squares crystal fractionation models for Mt Sefrit samples

Parent	Daughter	Melt (wt%)	Plag	Oliv	Cpx	Ilm	Σ(residual)^2
82-046	82-106	81·56	11·50	–0·87	6·94	–0·32	0·14
82-046	83-005	78·13	–18·60	9·61	12·26	–0·25	0·08
82-046	82-048	54·37	21·77	9·26	14·40	0·20	0·12
82-046	82-104	44·20	29·90	11·60	14·00	0·28	0·18

Whole-rock compositions are given in Table 4, mineral compositions are from microprobe analyses of gabbronorite samples from Mt Sefrit (Tepper, 1991). Negative values indicate mineral accumulation in the daughter rock.

Similarly, decreasing the amount of crystallization or M_a/M_c slightly improves the REE results, but significantly worsens the fit for Rb, Sr, Ba, and $^{87}Sr/^{86}Sr$. An alternative explanation for the REE and ε_{Nd} data is that, owing to the slow diffusion of REE, the phyllite xenoliths failed to equilibrate fully with the host magma. Isotopic equilibration between mafic enclaves and granites is slower for Nd than for Sr (Holden *et al.*, 1987). A similar situation would be expected for exchange involving wallrock xenoliths. At Mt Sefrit, if it is assumed that only 20% of the phyllite REE was contributed to the host magma during AFC, calculated REE content and ε_{Nd} are in agreement with other trace elements and Sr isotope systematics. The presence of unequilibrated wallrock material in two-pyroxene diorite 83-005 could also explain why that sample has higher $^{87}Sr/^{86}Sr$ and lower ε_{Nd} than the more evolved quartz diorite 82-104. Alternatively, these two samples could lie on different liquid lines of descent, but this would require that 83-005 formed under conditions where M_a/M_c was significantly greater or where the assimilant was different.

Crystallization of the Mt Sefrit parent magma probably took place over a range of depths within the crust and mantle, but most of the differentiation that produced the various rock types probably occurred within 10 km of the surface. Involvement of Darrington Phyllite, which has an estimated thickness of 3 km (Misch, 1966), implies differentiation within several kilometers of the present level of exposure (3–5 km on the basis of hornblende geobarometry on adjacent granitoids).

Low-K series differentiation

LKS samples were analyzed from composite plutons at Whatcom Pass and Copper Lake, both of which contain rocks ranging from gabbro to quartz diorite. In both cases there is a progression toward more differentiated compositions with decreasing age, and sharp contacts between rock types indicate that most of the petrologic diversity was generated below the level of emplacement. The Whatcom Pass samples show very limited variation in trace element abundances (Fig. 4d); they may represent a group of similar magmas rather than a comagmatic series and will not be discussed here. In contrast, the Copper Lake samples display systematic variations in major element, trace element, and isotopic composition that suggest they are related by extensive high-pressure differentiation and assimilation.

Differentiation of Copper Lake magmas at upper-mantle–lower-crustal pressures is indicated by several lines of evidence:

(1) The diorites and quartz diorites have low *mg*-numbers (0·45–0·37), but display limited SiO_2 enrichment, suggesting fractionation dominated by pyroxene rather than olivine or amphibole. In an experimental study of compositionally similar LKOT, Bartels *et al.* (1991) found clinopyroxene on the liquidus at pressures >10 kbar, whereas at lower pressures clinopyroxene follows, and is subordinate to, olivine and plagioclase.

(2) Sr increases with differentiation, indicating $D_{Sr}<1$. This requires that plagioclase constitute <50% of the crystallizing assemblage (assuming $D^{Sr}_{plag} \geqslant 2$; Blundy & Wood, 1991), which is also consistent with the absence of significant negative Eu anomalies among these samples. In the experiments of Bartels *et al.* (1991), plagioclase accounted for <50% of the minerals present only in runs at $P \geqslant$ 10 kbar.

(3) Relative to the gabbros, diorites and quartz diorites at Copper Lake show extreme depletion in Cr and Ni, but little change in Sc. Compositions of amphibole separates (Table 3, Nos 8 and 9) confirm that low Cr and high Sc are characteristics of the melt and not artifacts of crystal accumulation. These data are consistent with removal of Cr spinel at pressures >10 kbar (Bartels *et al.*, 1991) and/or extensive pyroxene + plagioclase fractionation at 1250°C [where $\overline{D}_{Sc} \sim 1$ for 50:50 plag + cpx, based upon data of Irving (1978)].

(4) Major element variation among the different

rock types at Copper Lake (excluding pegmatite 88-034) cannot be modeled by low-pressure fractionation. All attempts to derive diorites or quartz diorites from the gabbros by removal and/or addition of plagioclase, pyroxene, amphibole, and/or ilmenite (using a range of mineral compositions from microprobe analyses of Copper Lake samples) yielded $\Sigma R^2 > 4$ and/or geologically implausible phase proportions.

Extensive fractionation is indicated by variation in incompatible trace elements (Ba, Th, Nb, LREE), which average 50–150% higher in the diorites than in the gabbros, and 50–70% higher in the quartz diorites than in the diorites. The variation between gabbro and diorite is accompanied by an increase in $^{87}Sr/^{86}Sr_i$ and decrease in $\varepsilon_{Nd(0)}$, indicating that differentiation was an open system process. However, no change in isotopic composition accompanies trace element variation between diorite and quartz diorite (Table 5). Three possible scenarios could account for this apparent decoupling of trace element and isotopic variation: (1) the diorites originated from an isotopically different mantle source and are not directly related to the gabbros; (2) M_a/M_c was high enough during differentiation that the diorites had already reached the composition of the assimilant and there was no further change in isotopic composition with fractionation; (3) assimilation and crystallization were separated in time and/or space, as might occur if the magma moved out of contact with the contaminant before the later stages of differentiation, or if heat and mass transfer were decoupled (Grove *et al.*, 1988). Explanation (1) is possible, but discounts the close temporal and spatial relationships between gabbro and diorite at Copper Lake, and their overall petrologic similarity. The other two scenarios are examined below.

Modeling to constrain M_a/M_c and the composition of the assimilant is based on the assumptions that differentiation from gabbro to diorite involved clinopyroxene, plagioclase, and spinel, that the proportions of these phases was between 47:47:6 and 62:31:7, and that the amount of crystallization was between 30 and 70%. These constraints are imposed by the geochemical arguments outlined above and by the experimental data of Bartels *et al.* (1991). Given these constraints, one can specify M_a/M_c, melt fraction, and the fractionating assemblage, and then calculate the assimilant composition required to produce the observed trace element and/or isotopic variation. Using average compositions for gabbro, diorite, and quartz diorite, the results of this modeling indicate that scenario (2) above, in which the lack of isotopic variation between diorite and quartz diorite is attributed to isotopic equilibration with the assimilant, is possible only if $M_a/M_c > 0{\cdot}95$. Based on thermodynamic modeling, Reiners *et al.* (1995) suggested that under some conditions $M_a/M_c > 1$ may be typical during the early stages of basalt-crust contamination. The calculated assimilant in this case (Table 9) is LREE depleted ($La/Yb_N = 0{\cdot}5$–$0{\cdot}7$; $HREE_N \sim 5$–6), with a positive Eu anomaly. At any $M_a/M_c < 0{\cdot}95$ an assimilant with $\varepsilon_{Nd} = +5$ would have insufficient isotopic leverage to account for the 1·5 ε_{Nd} decrease between gabbro and diorite. This conclusion is insensitive to choice of melt fraction, because successful modeling of incompatible element abundances requires that any decrease in melt fraction be compensated by lower levels of incompatible trace elements in the assimilant, and this has the effect of reducing its influence on Nd isotopic variation.

In the third scenario above, if decoupling of trace element and isotopic variation results from loss of contact with the assimilant, the second stage of differentiation (diorite to quartz diorite) can be successfully modeled by 40% fractional crystallization of clinopyroxene, plagioclase, spinel, and zircon. However, without direct knowledge of the assimilant, the earlier differentiation–assimilation history (gabbro to diorite) is not tightly constrained. If we assume a contaminant with $^{87}Sr/^{86}Sr = 0{\cdot}7040$ and $\varepsilon_{Nd} = +4$ (averages for Chilliwack granitoids and MKS gabbros, and perhaps representative of local lower crust–upper mantle), $M_a/M_c > 0{\cdot}8$ is required. Model assimilants in this case (Table 9) have characteristics that might be expected of a plagioclase-rich gabbroic cumulate: relatively flat REE patterns ($La/Yb_N = 0{\cdot}8$–$2{\cdot}5$; $HREE_N \sim 5$–6) with $Eu/Eu^* = 1{\cdot}1$–$1{\cdot}8$, 400–700 p.p.m. Sr, and <50 p.p.m. Cr, Ni, and Sc. Other contaminant compositions are of course possible, and lower M_a/M_c is predicted if the assimilant has higher $^{87}Sr/^{86}Sr$ and lower ε_{Nd}. However, $M_a/M_c < 0{\cdot}5$ would require an assimilant with $^{87}Sr/^{86}Sr > 0{\cdot}7042$ and $\varepsilon_{Nd} < 3{\cdot}5$, and isotopic data for Chilliwack granitoids and gabbros offer no evidence of such material in the deep crust or upper mantle beneath the North Cascades.

SUMMARY AND CONCLUSIONS

Lithologically diverse gabbro and diorite plutons comprise ~2% of the exposed area of the Chilliwack and are broadly similar to mafic stocks in other I-type Cordilleran batholiths. Interpluton petrologic diversity in the Chilliwack can be attributed to three

Table 9: Characteristics of model assimilant required to account for trace element and isotopic variation between Copper Lake gabbro and diorite for selected values of M_a/M_c, melt fraction, and mineral proportions in the crystallizing assemblage

M_a/M_c:	0·95	0·80	0·50	0·50	0·50
Melt fraction:	0·6	0·7	0·7	0·7	0·5
cpx:pl:sp:	65:29:6	65:29:6	65:29:6	47:47:6	65:29:6
Calculated assimilant characteristics					
La_N	3·40	11·0	36·0	37·0	10·5
La/Yb_N	0·65	1·80	3·60	4·60	1·81
Eu/Eu*	1·13	1·13	1·23	1·40	1·27
Sr (p.p.m.)	408	410	470	900	350
Ba (p.p.m.)	18	27	55	75	0
Sc (p.p.m.)	32	34	45	32	38
$^{87}Sr/^{86}Sr$	0·7038	0·7040	0·7048	0·7042	0·7044
ε_{Nd}	+5·0	+4·0	+3·3	+3·3	+2·0

factors: (1) chemical and isotopic differences in mantle source regions; (2) variation in degree of melting; (3) dissimilar paths of magma evolution in the mantle and crust. In contrast, study of composite plutons indicates that intrapluton diversity is largely the result of multiple intrusion of related magmas that in some cases may have differentiated from a common parent.

Differences in mantle source composition are reflected in division of Chilliwack gabbros into a medium-K series (MKS) and a low-K series (LKS). The former are compositionally similar to calc-alkaline basalts and basaltic andesites (CAB) from the Cascades and other arcs. Inverse REE modeling indicates the MKS source was LREE enriched ($La/Yb_N \sim 2$) and contained no residual garnet. MKS samples display LILE enrichment and HFSE depletion characteristic of many arc magmas, and in this regard are distinct from OIB-like basalts in the Southern Washington Cascades (SWC) (Leeman *et al.*, 1990). Greater HFSE depletions in Chilliwack samples may reflect a more compressional setting, leading to enhanced interaction with mantle wallrock during magma ascent (Kelemen *et al.*, 1990). In addition, however, greater involvement of a slab-derived component is indicated by $Ba/La = 23–37$ in MKS samples vs $Ba/La < 18$ in most SWC lavas. Among Cascade samples in general the 'arc signature' appears more pronounced in pre-Miocene rocks (Chilliwack samples; Leeman *et al.*, 1990; Fig. 5) and in rocks from the ends of the arc (Leeman *et al.*, 1990), suggesting that variation in slab involvement could be temporal as well as spatial, perhaps reflecting changes in subduction rate (Wells *et al.*, 1984) and/or segmentation of the slab (Guffanti & Weaver, 1988).

Chilliwack LKS gabbros have many of the distinctive chemical features of low-K olivine tholeiites (LKOT) found in the Southern Cascades and Basin and Range (McKee *et al.*, 1983; Hart *et al.*, 1984; Bacon, 1990; Leeman *et al.*, 1990). The LKS gabbros are less primitive, but both rock types are characterized by high Al_2O_3, CaO, Na_2O/K_2O, and Sc, and by low LILE and La/Yb_N. Many of these traits point to increased clinopyroxene component in the melt, and Clynne (1993) has suggested they reflect melting of LILE-depleted continental lithosphere that had been metasomatically enriched in pyroxene (Irving, 1980). Low La/Yb_N suggests that garnet was not residual in the LKS source, and the higher $\varepsilon_{Nd(0)}$ of LKS gabbros (relative to MKS) suggests that lower La/Yb_N was a long-lived characteristic of the source. Guffanti *et al.* (1990) recognized that the same mantle source and/or processes that produced LKOT in the Basin and Range must also exist or operate within the Lassen segment of the Cascade arc; similarities between LKS gabbros and LKOT would extend this conclusion to the northern end of the arc. In addition, because Miocene–Recent LKOT are found only in areas of active extension, a similar stress regime is implied in the North Cascades at 35 Ma. Crustal extension at this time has been suggested by Wells *et al.* (1984) and could account for ascent of LKS magmas through the crust with little modification.

Variation in degree of melting (9–27%) of a spinel lherzolite source can account for differences in La/Yb_N between separate MKS plutons. In contrast, the

fact that all samples from any individual pluton have similar La/Yb_N suggests that each stock represents a group of closely related magmas, in some cases differentiates of a common parent. Evolution of individual magma batches was strongly influenced by depth of crystallization. At Mt Sefrit, MKS differentiation occurred primarily through removal of olivine, plagioclase, and pyroxene at mid- to upper-crustal levels, accompanied by minor wallrock assimilation ($M_a/M_c \sim 0{\cdot}2$). Magma evolution in this case is marked by SiO_2 enrichment, decreases in Sr, Cr, Ni, and Eu/Eu*, but no significant change in La/Yb_N. In contrast, AFC modeling of LKS differentiation at Copper Lake indicates crystallization dominated by clinopyroxene + plagioclase ± Cr-spinel, implying pressures >10 kbar (Bartels *et al.*, 1991). The nature of the assimilant is poorly constrained, but $M_a/M_c > 0{\cdot}5$ is suggested by Sr isotopic data. Differentiation in this case is characterized by limited increase in SiO_2, higher Sr and La/Yb_N, negligible change in Eu/Eu*, and extreme Cr and Ni depletion.

In a companion study, Tepper *et al.* (1993) proposed that Chilliwack granitoids formed by partial melting of mafic lower crust having trace element and isotopic characteristics of the exposed mafic plutons. The present work, by documenting the geochemical similarities between these mafic plutons and Miocene–Recent Cascade basaltic lavas, confirms that mafic magmas present before (as the source) and during production of calc-alkaline granitoids included a range of low- and medium-K arc basalts and their differentiates.

ACKNOWLEDGEMENTS

This paper represents part of a University of Washington Ph.D. dissertation, and has benefited from numerous discussions with I. S. McCallum, A. J. Irving, B. K. Nelson, and the late Peter Misch. I would also like to thank R. Tabor and R. Haugerud (USGS) for field support and for sharing unpublished data, M. Clynne (USGS) for sharing unpublished data, J. Sparks, H. R. Naslund, and D. Mittlefehldt for chemical analyses, P. Kelemen, A. Buddington, M. Thurber, C. Anderson, and J. Emery for discussion and assistance in the field, and J. Blundy and C. Barnes for thorough and helpful reviews of this paper. Logistical support and permission to collect samples were kindly provided by personnel of North Cascades National Park. Partial funding was provided by grants from the Washington Department of Natural Resources, the Department of Geological Sciences Graduate Research Fund, and the University of Washington Graduate Research Fund.

REFERENCES

Aoki, K., 1971. Petrology of mafic inclusions from Itinome-gata, Japan. *Contributions to Mineralogy and Petrology* **30,** 314–331.

Bacon, C. R., 1990. Calc-alkaline, shoshonitic, and primitive tholeiitic lavas from monogenetic volcanoes near Crater Lake, Oregon. *Journal of Petrology* **31,** 135–166.

Bartels, K. S., Kinzler, R. J. & Grove, T. L., 1991. High pressure phase relations of primitive high-alumina basalts from Medicine Lake volcano, northern California. *Contributions to Mineralogy and Petrology* **108,** 253–270.

Bateman, P. C., 1983. A summary of critical relations in the central part of the Sierra Nevada batholith, California, U.S.A. In: Roddick, J. A. (ed.) *Circum-Pacific Plutonic Terranes. Geological Society of America, Memoir* **159,** 241–254.

Beard, J. S. & Day, H. W., 1988. Petrology and emplacement of reversely zoned gabbro–diorite plutons in the Smartville Complex, Northern California. *Journal of Petrology* **29,** 965–995.

Blundy, J. D. & Sparks, R. S. J., 1992. Petrogenesis of mafic inclusions in granitoids of the Adamello Massif, Italy. *Journal of Petrology* **33,** 1039–1104.

Blundy, J. D. & Wood, B. J., 1991. Crystal-chemical controls on the partitioning of Sr and Ba between plagioclase feldspar, silicate melts, and hydrothermal solutions. *Geochimica et Cosmochimica Acta* **55,** 193–210.

Boynton, W. V., 1984. Cosmochemistry of the rare earth elements: meteorite studies. In: Henderson, P. (ed.) *Rare Earth Element Geochemistry*. New York: Elsevier, pp. 63–114.

Brown, E. H., Blackwell, D. L., Christenson, B. W., Frasse, F. I., Haugerud, R. A., Jones, J. T., Leiggi, P. L., Morrison, M. L., Rady, P. M., Reller, G. J., Sevigny, J. H., Silverberg, D. L., Smith, M. T., Sondergaard, J. N. & Ziegler, C. B., 1987. *Geologic map of the northwest Cascades, Washington*. Boulder, CO: Geological Society of America, Map and Chart Series MC-61, 10 pp.

Clynne, M. A., 1993. Geologic studies of the Lassen volcanic center, Cascade Range, California. Ph.D. Dissertation, University of California, Santa Cruz, 404 pp.

DePaolo, D. J., 1981. Trace element and isotopic effects of combined wallrock assimilation and fractional crystallization. *Earth and Planetary Science Letters* **53,** 189–202.

Eberz, G. W. & Nicholls, I. A., 1990. Chemical modification of enclave magma by post-emplacement crystal fractionation, diffusion and metasomatism. *Contributions to Mineralogy and Petrology* **104,** 47–55.

Erickson, E. H., Jr, 1977. Petrology and petrogenesis of the Mount Stuart batholith—plutonic equivalent of the high-alumina basalt association? *Contributions to Mineralogy and Petrology* **60,** 183–207.

Fabries, J., Conquere, F. & Arnaud, G., 1984. The mafic silicates in the Saint Quay-Portrieux gabbro–diorite intrusion: crystallization conditions of a calc-alkaline pluton. *Bulletin de Minéralogie* **107,** 715–736.

Fourcade, S. & Allègre, C. J., 1981. Trace elements behavior in granite genesis: a case study of the calc-alkaline plutonic association from the Querigut Complex (Pyrenees, France). *Contributions to Mineralogy and Petrology* **76,** 177–195.

Fujimaki, H., Tatsumoto, M. & Aoki, K., 1984. Partition coefficients of Hf, Zr, and REE between phenocrysts and groundmasses. *Journal of Geophysical Research* **89,** B662–B672.

Green, T. H. & Pearson, N. J., 1985. Rare earth element partitioning between clinopyroxene and silicate liquid at moderate to high pressure. *Contributions to Mineralogy and Petrology* **91,** 24–36.

Grove, T. L., Kinzler, R. J., Baker, M. B., Donnelly-Nolan, J. M. & Lesher, C. E., 1988. Assimilation of granite by basaltic magma at Burnt Lava flow, Medicine Lake volcano, northern California: decoupling of heat and mass transfer. *Contributions to Mineralogy and Petrology* **99,** 320–343.

Guffanti, M. & Weaver, C. S., 1988. Distribution of late Cenozoic volcanic vents in the Cascade Range: volcanic arc segmentation and regional tectonic considerations. *Journal of Geophysical Research* **93,** 6513–6529.

Guffanti, M., Clynne, M. A., Smith, J. G., Muffler, L. P. J. & Bullen, T. D., 1990. Late Cenozoic volcanism, subduction, and extension in the Lassen region of California, southern Cascade Range. *Journal of Geophysical Research* **95,** 19453–19464.

Halliday, A. N., Fallick, A. E., Dickin, A. P., Mackenzie, A. B., Stephens, W. E. & Hildreth, W., 1983. The isotopic and chemical evolution of Mount St. Helens. *Earth and Planetary Science Letters* **63,** 241–256.

Harrison, W. J., 1981. Partitioning of REE between minerals and coexisting melts during partial melting of a garnet lherzolite. *American Mineralogist* **66,** 242–259.

Hart, W. K., Aronson, J. L. & Mertzman, S. A., 1984. Areal distribution and age of low-K, high-alumina olivine tholeiite magmatism in the northwestern Great Basin. *Geological Society of America Bulletin* **95,** 186–195.

Helz, R. T., 1976. Phase relations of basalts in their melting ranges at $PH_2O = 5$ kbar. Part II. Melt compositions. *Journal of Petrology* **17,** 139–193.

Hofmann, A. W. & Feigenson, M. D., 1983. Case studies on the origin of basalt I. Theory and reassessment of Grenada basalts. *Contributions to Mineralogy and Petrology* **84,** 382–389.

Holden, P., Halliday, A. N. & Stephens, W. E., 1987. Neodymium and strontium isotope content of microdiorite enclaves points to mantle input in granitoid production. *Nature* **330,** 53–56.

Holland, T. & Blundy, J., 1994. Non-ideal interactions in calcic amphiboles and their bearing on amphibole–plagioclase thermometry. *Contributions to Mineralogy and Petrology* **116,** 443–447.

Hughes, S. S., 1990. Mafic magmatism and associated tectonism of the central High Cascades Range, Oregon. *Journal of Geophysical Research* **95,** 19623–19638.

Irvine, T. N. & Baragar, W. R. A., 1971. A guide to the classification of the common volcanic rocks. *Canadian Journal of Earth Sciences* **8,** 523–548.

Irving, A. J., 1978. A review of experimental studies of crystal/liquid trace element partitioning. *Geochimica et Cosmochimica Acta* **42,** 743–770.

Irving, A. J., 1980. Petrology and geochemistry of composite ultramafic xenoliths in alkalic basalts and implications for magmatic processes within the mantle. *American Journal of Science* **280-A,** 389–426.

Irving, A. J. & Frey, F. A., 1984. Trace element abundances in megacrysts and their host basalts: constraints on partition coefficients and megacryst genesis. *Geochimica et Cosmochimica Acta* **48,** 1201–1221.

Jaques, A. L. & Green, D. H., 1980. Anhydrous melting of peridotite at 0–15 kbar pressure and the genesis of tholeiitic basalts. *Contributions to Mineralogy and Petrology* **73,** 287–310.

Kelemen, P. B., Johnson, K. T. M., Kinzler, R. J. & Irving, A. J., 1990. High field strength element depletion in arc basalts due to mantle–magma interaction. *Nature* **345,** 521–524.

Larsen, E. S., Jr, 1948. Batholith and associated rocks of Corona, Elsinore, and San Luis Rey quadrangles, southern California. *Geological Society of America, Memoir* **29,** 182 pp.

Leake, B. E., 1978. Nomenclature of amphiboles. *Mineralogical Magazine* **42,** 533–563.

Leeman, W. P., Smith, D. R., Hildreth, W., Palacz, Z. & Rogers, N., 1990. Compositional diversity of Late Cenozoic basalts in a transect across the Southern Washington Cascades: implications for subduction zone magmatism. *Journal of Geophysical Research* **95,** 19561–19582.

McGroder, M. F., 1991. Reconciliation of two-sided thrusting, burial metamorphism, and diachronous uplift in the Cascades of Washington and British Columbia. *Geological Society of America Bulletin* **103,** 189–209.

McKay, G. A., 1989. Partitioning of rare earth elements between major silicate minerals and basaltic melts. *Mineralogical Society of America, Reviews in Mineralogy* **21,** 45–77.

McKee, E. H., Duffield, W. A. & Stern, R. J., 1983. Late Miocene and early Pliocene basaltic rocks and their implications for crustal structure, northeastern California and south-central Oregon. *Geological Society of America Bulletin* **94,** 292–304.

Miller, D. F., Langmuir, C. H., Goldstein, S. L. & Franks, A. L., 1992. The importance of parental magma composition to calc-alkaline and tholeiitic evolution: evidence from Umnak Island in the Aleutians. *Journal of Geophysical Research* **97,** 321–343.

Miller, F. S., 1937. Petrology of the San Marcos Gabbro, Southern California. *Geological Society of America Bulletin* **48,** 1197–1226.

Minster, J. F. & Allègre, C. J., 1978. Systematic use of trace elements in igneous processes, Part III: inverse problem of batch partial melting in volcanic suites. *Contributions to Mineralogy and Petrology* **68,** 37–52.

Misch, P., 1966. Tectonic evolution of the Northern Cascades of Washington state. In: Gunning, H. C. (ed.) *Tectonic History and Mineral Deposits of the Western Cordillera. Canadian Institute of Mining and Metallurgy Special Volume* **8,** 101–148.

Miyashiro, A., 1974. Volcanic rocks series in island arcs and active continental margins. *American Journal of Science* **274,** 321–355.

Mullan, H. S. & Bussell, M. A., 1977. The basic rock series in batholithic associations. *Geological Magazine* **114,** 265–280.

Phinney, W. C. & Morrison, D. A., 1990. Partition coefficients for calcic plagioclase: implications for Archean anorthosites. *Geochimica et Cosmochimica Acta* **54,** 1639–1654.

Regan, P. F., 1985. The early basic intrusions. In: Pitcher, W. S., Atherton, M. P., Cobbing, E. J. & Beckinsale, R. D. (eds) *Magmatism at a Plate Edge—the Peruvian Andes.* Glasgow: Blackie, pp. 72–89.

Reid, J. B., Jr, Evans, O. C. & Fates, D. G., 1983. Magma mixing in granitic rocks of the central Sierra Nevada, California. *Earth and Planetary Science Letters* **66,** 243–261.

Reiners, P. W., Nelson, B. K. & Ghiorso, M. S., 1995. Assimilation of felsic crust by basaltic magma: thermal limits and extents of crustal contamination of mantle-derived magmas. *Geology* **23,** 563–566.

Richards, T. A., 1971. Plutonic rocks between Hope, B.C., and the 49th Parallel. Ph.D. Dissertation, University of British Columbia, Vancouver, 178 pp.

Rickwood, P. C., 1989. Boundary lines within petrologic diagrams which use oxides of major and minor elements. *Lithos* **22,** 247–263.

Shimizu, H., Sangen, K. & Masuda, A., 1982. Experimental study on rare-earth element partitioning in olivine and clinopyroxene

formed at 20 kbar for basaltic systems. *Geochemical Journal* **16**, 107–117.

Sisson, T. W. & Grove, T. L., 1993. Temperatures and H_2O contents of low-MgO high alumina basalts. *Contributions to Mineralogy and Petrology* **113**, 167–184.

Sisson, T. W. & Layne, G. D., 1993. H_2O in basalt and basaltic andesite glass inclusions from four subduction-related volcanoes. *Earth and Planetary Science Letters* **117**, 619–635.

Sun, S. S. & McDonough, W. F., 1989. Chemical and isotopic systematics of oceanic basalts: implications for mantle composition and processes. In: Saunders, A. D. & Norry, M. J. (eds) *Magmatism in the Ocean Basins. Geological Society of London Special Publication* **42**, 313–315.

Tepper, J. H., 1991. Petrology of mafic plutons and their role in granitoid genesis, Chilliwack batholith, North Cascades, Washington. Ph.D. Dissertation, University of Washington, Seattle, 307 pp.

Tepper, J. H., Nelson, B. K., Bergantz, G. W. & Irving, A. J., 1993. Petrology of the Chilliwack batholith, North Cascades, Washington: generation of calc-alkaline granitoids by melting of mafic lower crust with variable water fugacity. *Contributions to Mineralogy and Petrology* **113**, 333–351.

Ulmer, P., 1989. The dependence of the Fe^{2+}–Mg cation-partitioning between olivine and basaltic liquid on pressure, temperature, and composition. *Contributions to Mineralogy and Petrology* **101**, 261–273.

Vance, J. A., 1965. Zoning in igneous plagioclase: patchy zoning. *Journal of Geology* **73**, 636–651.

Walawender, M. J. & Smith, T. E., 1979. Geochemical and petrologic evolution of the basic plutons of the Peninsular Ranges batholith, southern California. *Journal of Geology* **88**, 233–242.

Watson, E. B. & Green, T. H., 1981. Apatite/liquid partition coefficients for the rare earth elements and strontium. *Earth and Planetary Science Letters* **56**, 405–421.

Wells, P. R. A., 1977. Pyroxene thermometry in simple and complex systems. *Contributions to Mineralogy and Petrology* **62**, 129–139.

Wells, R. E., Engebretson, D. C., Snavely, P. D., Jr & Coe, R. S., 1984. Cenozoic plate motions and the volcano-tectonic evolution of western Oregon and Washington. *Tectonics* **3**, 275–294.

RECEIVED MAY 25, 1994
REVISED TYPESCRIPT ACCEPTED JUNE 18, 1996

APPENDIX A: ANALYTICAL METHODS

Mineral analyses

Major and minor elements were analyzed on the University of Washington Geology Department JEOL 733 electron microprobe using natural standards, 15 kV accelerating voltage, a focused 5–10 mm beam, and a 20–30 nA cup current. Data were reduced on-line with a Bence–Albee correction program. Trace element analyses of amphibole were by instrumental neutron activation analysis (INAA) at JSC–NASA (D. Mittlefehldt, analyst).

Whole-rock analyses

Major and trace element analyses by inductively coupled plasma emission spectrometry (ICP-ES) were performed on a Baird PS-1 48 channel spectrometer at the University of Washington. Major elements were determined on 0·1 g of rock powder fused with lithium metaborate and dissolved in dilute nitric acid. Trace element analytical solutions were prepared by digestion of 0·5 g of rock powder in an HF–HNO_3–$HClO_4$ mixture, followed by evaporation and redissolution in dilute HCl. REE were determined on an aliquot of this solution following separation and preconcentration by cation exchange column. Further details have been given by Tepper *et al.* (1993). Based on analysis of standards, relative analytical uncertainties are estimated as follows: Si, Al ($\leqslant$1%); Fe, Mg, Ca (~2%); Na (3–5%); REE (2–5%); Nb and Li (10–15%); K and other trace elements ($\leqslant$5%). Trace element analyses by inductively coupled plasma mass spectrometry (ICP-MS) were performed at Union College on a VG PQ2+. Preparation of 0·1 g samples was by fusion with lithium metaborate or by acid digestion in an HF–HNO_3 mixture, followed in both cases by dissolution in dilute HNO_3 containing an internal standard. All samples were prepared in duplicate and run against a range of natural standards including NBS688, NBS278, and ARHCO-1. Data reduction, including corrections for drift in internal standards and calibration curves, was with VGFIX (K. Hollocher, personal communication, 1994). Based on replicate analyses of standards, relative analytical precision for ICP-MS data is estimated at 1–4% for REE; $\leqslant$5% for Sc, V, Cr, Ni, Sr, Y, Ba, Hf; $\leqslant$10% for Rb, Nb, Zr, Pb, Th, U; and ~20% for Cs, Ta and Th < 1 p.p.m. Comparison of data for three samples analyzed by both ICP-ES and ICP-MS indicates that agreement between these methods is within 5% for Sr and Ba; within 10% for REE, Cr, and V; and within 15% for other trace elements except Sc and Ni (~20%). Rb determinations by isotope dilution were performed at the University of Washington using a VG Sector mass spectrometer; agreement between these data and those obtained by ICP-MS on the same samples is within 6%. Major element analyses by direct current plasma spectrometry (DCP) were performed in duplicate at SUNY–Binghampton on 0·1 g samples that were fused with lithium metaborate, dissolved in dilute HCl containing an internal standard, and run against natural standards NBS688, NBS278, and ARHCO-1. Major element analyses by X-ray fluorescence (XRF) were performed at Stanford University (J. Sparks, analyst). For all samples loss-on-ignition was measured by weighing 1 g of powder before and after firing at 1050°C for 1 h. Ferrous iron was determined volumetrically.

Isotopic analyses

Sr and Nd isotopic analyses were performed at the University of Washington using a VG Sector mass spectrometer. Samples (200 mg) were digested in an HF–$HClO_4$ mixture and then redissolved in HCl. Following column separation, Sr isotopic composition was determined on ~500 ng of sample loaded on a single Ta filament. Nd was run as Nd^+ on ~500 ng sample loaded onto the side filament of a Re triple filament. Additional details have been given by Tepper *et al.* (1993).

APPENDIX B: DISTRIBUTION COEFFICIENTS USED IN TRACE ELEMENT MODELING

	olivine	opx	cpx	garnet	spinel	plag	ilmenite	apatite
Reference:	1,2	2,3	3,4,5	6,7	1,2,7	1,8,9,10	1	11
La	0·00001	0·003	0·09	0·06	0·0006	0·15	0·01	7·0
Ce	0·00002	0·005	0·13	0·09	0·0006	0·11	0·01	9·0
Pr	0·00005	0·006	0·18	0·15	0·0006	0·09	—	—
Nd	0·0001	0·01	0·26	0·23	0·0006	0·08	0·01	11·0
Sm	0·0006	0·02	0·50	0·52	0·0007	0·06	0·01	13·0
Eu	0·0009	0·03	0·60	0·76	0·0008	0·80	0·01	14·0
Gd	0·001	0·04	0·69	1·2	0·0009	0·05	0·02	13·0
Tb	0·002	0·05	0·75	1·7	0·001	0·04	—	—
Dy	0·004	0·06	0·83	2·3	0·001	0·04	0·02	11·0
Ho	0·005	0·07	0·84	3·2	0·002	0·04	0·03	10·0
Er	0·009	0·09	0·85	4·0	0·003	0·03	—	—
Yb	0·023	0·12	0·86	6·6	0·004	0·03	0·05	7·0
Lu	0·037	0·15	0·85	7·8	0·005	0·03	0·10	6·0
Rb	0·01	0·01	0·01	—	0·01	0·03	0·01	0·01
Sr	0·01	0·01	0·1	—	0·05	2·2	0·01	2·0
Ba	0·01	0·01	0·01	—	0·05	0·3	0·05	0·05
Sc	0·3	1·1	1·5	—	0·05	0·05	3·	0·05
Cr	1·0	8·0	15·0	—	50·0	0·05	6·0	0·05
Ni	15·0	2·0	1·5	—	10·0	0·05	20·0	1·0

Sources: 1, Irving (1978); 2, Kelemen *et al.* (1990); 3, Irving & Frey (1984); 4, Shimizu *et al.* (1982); 5, Green & Pearson (1985); 6, Fujimaki *et al.* (1984); 7, Miller *et al.* (1992); 8, Phinney & Morrison (1990); 9, McKay (1989); 10, Blundy & Wood (1991); 11, Watson & Green (1981).